JAMES | Journal of Advances in Modeling Earth Systems

RESEARCH ARTICLE
10.1029/2019MS001650

Surface-Atmosphere Coupling Scale, the Fate of Water, and Ecophysiological Function in a Brazilian Forest

Ian T. Baker[1], A. Scott Denning[1], Don A. Dazlich[1], Anna B. Harper[2], Mark D. Branson[1], David A. Randall[1], Morgan C. Phillips[1], Katherine D. Haynes[1], and Sarah M. Gallup[1]

[1]Atmospheric Science Department, Colorado State University, Fort Collins, CO, USA, [2]College of Engineering, Mathematics, and Physical Sciences, University of Exeter, Exeter, England

Key Points:
- Ecophysiological function during seasonal drought is dependent upon storage and availability of rainfall that falls during the wet season
- The scale of coupling between land and atmosphere strongly influences this "fate of water" in simulations
- Simulations tend toward "water limitation" or "light limitation" depending on this scale of coupling

Correspondence to:
I. T. Baker,
ian.baker@colostate.edu

Citation:
Baker, I. T., Denning, S., Dazlich, D., Harper, A., Branson, M., Randall, D. A., et al. (2019). Surface-atmosphere coupling scale, the fate of water, and ecophysiological function in a Brazilian forest. *Journal of Advances in Modeling Earth Systems*, *11*, 2523–2546. https://doi.org/10.1029/2019MS001650

Received 4 FEB 2019
Accepted 16 JUL 2019
Accepted article online 23 JUL 2019
Published online 5 AUG 2019

Abstract Tropical South America plays a central role in global climate. Bowen ratio teleconnects to circulation and precipitation processes far afield, and the global CO_2 growth rate is strongly influenced by carbon cycle processes in South America. However, quantification of basin-wide seasonality of flux partitioning between latent and sensible heat, the response to anomalies around climatic norms, and understanding of the processes and mechanisms that control the carbon cycle remains elusive. Here, we investigate simulated surface-atmosphere interaction at a single site in Brazil, using models with different representations of precipitation and cloud processes, as well as differences in scale of coupling between the surface and atmosphere. We find that the model with parameterized clouds/precipitation has a tendency toward unrealistic perpetual light precipitation, while models with explicit treatment of clouds produce more intense and less frequent rain. Models that couple the surface to the atmosphere on the scale of kilometers, as opposed to tens or hundreds of kilometers, produce even more realistic distributions of rainfall. Rainfall intensity has direct consequences for the "fate of water," or the pathway that a hydrometeor follows once it interacts with the surface. We find that the model with explicit treatment of cloud processes, coupled to the surface at small scales, is the most realistic when compared to observations. These results have implications for simulations of global climate, as the use of models with explicit (as opposed to parameterized) cloud representations becomes more widespread.

1. Introduction

The South American tropics contain the largest evergreen broadleaf forest (EBF) on Earth. Estimates of total biomass vary (Avitabile et al., 2016; Saatchi et al., 2007), but the total is high, up to 10% of global aboveground biomass (Houghton et al., 2001). Relatively minor anomalies in large gross fluxes of photosynthesis (gross primary productivity, GPP) and total ecosystem respiration in the region have been linked to a significant influence on global atmospheric CO_2 growth rates (Gurney et al., 2008; Peylin et al., 2013; Rödenbeck et al., 2003; Wenzel et al., 2014) . Furthermore, forest behavior through seasonal wet-dry cycles in present-day climate as well as response to variability such as drought is poorly understood. This uncertainty is reflected in model simulations, seen in the spread of model predictions of atmospheric CO_2 concentration and strength (and even sign) of the land sink by the end of this century (e.g., Friedlingstein et al., 2006, 2014; Powell et al., 2013) as well as in the diversity of simulations of seasonality and amplitude of the present-day carbon cycle in the 15 members of the Multiscale Terrestrial Model Intercomparison Project (Huntzinger et al., 2018). It is therefore critical that we improve our understanding of surface-atmosphere interaction in tropical South America, with regard to physical processes as well as the discretization of these processes in numerical models.

Tropical evergreen forests in South America are warm throughout the year, and day length has low variability due to proximity to the equator. Seasonality is primarily imposed by gradients in rainfall characteristics in time and space as the Intertropical Convergence Zone oscillates north and south during the year (Fu et al., 1999; Horel et al., 1989; Nieto-Ferreira & Rickenbach, 2011). Precipitation variability can be described in terms of total annual rainfall combined with the length of dry season, which is generally described as the number of months in which precipitation is 100 mm or less (Goulden et al., 2004). In the wet Northwest rain is ample throughout the year, and each month in the "dry season" may still have 100-mm/month

precipitation or more. Moving to the south and east, annual total rainfall is less, and the dry season length can increase to up to 7 months. For EBF annual precipitation of ~1,700 mm/year generally defines the edge of EBF (Davidson et al., 2012), although forest boundary is not explicitly defined by precipitation (Malhi et al., 2006). Furthermore, the local environment can also be influenced by the characteristics of precipitation during dry and wet seasons. For example, the K34 tower near Manaus, in north central Brazil (Araújo, 2002), and Reserva Jaru (RJA; von Randow et al., 2004) 900 km to the south, have similar annual precipitation amount (de Gonçalves et al., 2013). However, at RJA the wettest months can have 450 mm of rain or more, and rain can be almost nonexistent in the dry season. The wet season rainfall atK34 is less than at RJA, and during drier months rainfall of almost 100 mm/month is not uncommon. These four factors (annual rainfall, dry season length, wet season precipitation intensity, and dry season rainfall occurrence), and the climatological variabilty around them, all contribute substantially to the nature of the exchanges of energy, water, and CO_2 between the surface and atmosphere.

The ecosystem can be thought of as functioning fundamentally within one of two archetypes, described as "environmental control" or "biophysical control" in da Rocha et al. (2009) and Costa et al. (2010). An environmentally controlled ecosystem is not water limited and will transpire at the potential rate, dependent upon incoming radiation, temperature, and vapor pressure deficit (VPD). One might think of this system as "light limited," in that an increase in insolation results in an increase in photosynthesis and transpiration. Where water is less plentiful, stomatal regulation by plants plays a larger role in regulating seasonal cycles of Bowen ratio and carbon flux. In these "biophysically controlled" or "water-limited" environments the canopy cannot maintain optimal function throughout the entire year, and plants will close stomates partially or completely as a water-saving mechanism. For simplicity, we will use light limited and water limited as descriptors hereafter. It is possible to classify individual sites as belonging to one endpoint or the other, but in reality it is likely that the shift from light to water limitation is relatively smooth as one moves along precipitation gradients from wetter regions in the north and west to hotter, more seasonal and relatively dry EBF regions to the south and east. Furthermore, it is also likely that an individual location can experience a shift in controlling mechanism during the annual cycle and in response to variability about the mean. Other factors such as nutrient cycles play a role in canopy behavior, but we believe (and the literature reflects) that water and light are the main controls (e.g., Bonan, 2016, Figure 24.6) on the annual cycles evaluated here. Costa et al. (2010) classified individual observation sites as light or water limited, but with few sites and relatively short observation periods it is likely that regional understanding of spatiotemporal control over canopy status and fluxes is incomplete.

The literature reflects these gaps in knowledge. Early coupled climate-carbon cycle models predicted that the Amazonian forest is fragile and would convert to savanna or grassland over the next century (Betts et al., 2004; Cox et al., 2000, 2004; Huntingford et al., 2008). Many of these simulations predicted a dry season temperature 2–3 °C warmer than observed during preindustrial/present-day simulations (Cox et al., 2004), which may suggest water limitation (closing stomates and an increase in Bowen ratio) in the model where light limitation was actually occurring in nature. As these simulations also predicted a dramatic decrease in EBF extent in tropical South America during the 21st century, it may be that stress was being unrealistically applied. More recent results (Cox et al., 2013; Good et al., 2013) have retreated from these earlier results somewhat and speculated that tropical forest dieback may not be as rapid and/or severe as originally predicted. However, it is notable that Good et al. (2013) attribute more resilient tropical forest to changes in climate in new simulations, not changes in simulated forest ecophysiology or land-atmosphere coupling. Saleska (2003) showed that multiple models predicted the seasonality of CO_2 flux *exactly wrong* at sites near Santarem, Brazil. Baker et al. (2008) showed similar behavior and were able to reproduce observed behavior by making the model soil deeper and modifying mechanisms used by roots to withdraw water from the soil. Some authors have reported basin-wide "greening-up" during dry seasons and droughts (Huete et al., 2006; Saleska et al., 2007, 2016) indicative of environmental control, yet these results have been challenged by others as artifacts of satellite retrieval (Morton et al., 2014) or errors in analysis (Samanta et al., 2010, 2011). Solar-induced fluorescence data explored by Lee et al. (2013) indicate a decrease in canopy productivity as the dry season progresses, indicative of increasing water stress, a finding supported by solar-induced fluorescence and column CO_2 data evaluated by Parazoo et al. (2013); however, these studies do not address the entirety of the South American EBF. In a study using data from multiple observation sites, Wu et al. (2017) reported that the photosynthetic capacity of leaves was maximized 1 to 2 months following leaf-out. Saleska et al. (2016) combined this finding with a reanalysis of the data of Morton et al. (2014) to reiterate their the-

ory of dry season green-up. Restrepo-Coupe et al. (2013) noted an inverse relationship (or no relationship) between precipitation at wet sites (light limitation), while sites to the south and east exhibited a correlation between rainfall and photosynthesis (water limitation). Baker et al. (2013) reproduced this behavior generally with a model, but Restrepo-Coupe et al. (2017) noted that many models are unable to do so. While quantitative understanding of spatiotemporal ecophysiology in response to seasonal and anomalous forcing is expanding, we do not consider the matter closed.

In this paper we will explore the extent to which model configuration and surface-atmosphere coupling scale influence which control mechanism (light or water limitation) exerts dominance over simulated fluxes. We will (1) evaluate how precipitation characterization, based on conventional General Circulation Model (GCM) parameterizations, change when explicit simulation of clouds and precipitation is used instead. We will (2) investigate the fate of water that falls as precipitation. Water can be evaporated directly off of leaves, or it can exceed canopy storage capacity and reach the ground. Once on the ground, water can infiltrate, where it may be available for transpiration at a later date (or lost to the system as subsurface runoff), or rainfall intensity may exceed infiltration capacity resulting in overland runoff. Finally, we will (3) investigate the variability in simulated ecosystem status and fluxes as a result of these mechanisms. We do this by comparing three configurations of a single-column model (SCM) with differing parameterizations of cloud and precipitation properties and coupling scale length at the surface. We employ these simulations over a single GCM grid cell containing the K83 tower site (Goulden et al., 2004; Miller et al., 2004, 2011) in the Tapajos River Nation Forest near Santarem, Brazil. Section 2 describes the observation site and models used. Section 3 presents results, and conclusions are shared in section 4.

2. Methods

2.1. Tapajos River National Forest Km 83 Site

The K83 site is located in a tropical forest of primarily evergreen and a few deciduous tree species located ~70 km south of Santarém in Pará State, Brazil. The site and instrumentation is described in Goulden et al. (2004). Mean annual precipitation for the years investigated (2001–2003) is ~1,660 mm/year (Baker et al., 2013; de Gonçalves et al., 2013), with a wet season from January–June and dry season from July–December. The amplitude of the monthly averaged radiation cycle is small (~50 W), with a peak during the dry season. Observed sensible (H) and latent heat (LE) fluxes have minimal annual variability as well, with peaks in both coincident with dry season radiation maximum, so that Bowen ratio is almost invariant through the year.

That the Bowen ratio does not increase during seasonal drought implies that the forest at this site does not enter a stressed condition when seasonal rains cease, contradictory to model simulations that suggest that photosynthesis is strongly water limited (Baker et al., 2008; Saleska, 2003). Saleska (2003) proposes that forest function is maintained by deep roots that have access to stored water. Baker et al., 2008 (2008, 2013) demonstrate that model simulations at K83 match observations better when model soil depth is extended (from a "traditional" value of ~3.5 m to 10 m), and the ability of roots to extract water is decoupled from fractional root concentration in model soil layers. In this way, the model (1) provides sufficient soil reservoir to store water from the water-rich wet season for use during seasonal drought and (2) plant roots can access water deep in the soil once surface layers are depleted (Jipp et al., 1998; Nepstad et al., 1994; Oliveira et al., 2005).

2.2. Models

We can express our hypotheses pertaining to ecophysiological function and land-atmosphere interactions as a series of equations. A model is a discretization and compilation of these hypotheses into a self-consistent body that can be evaluated against available observations as a test of their overall validity and can be customized for particular applications. Here, we are concerned with surface-atmosphere exchange and the scale of coupling between land and atmosphere, with specific interest in precipitation characteristics and its interaction with canopy processes and subsequent influence on the carbon cycle in EBF regions. Our ultimate interest is global models, but we will concentrate our analysis here on a single EBF grid cell, which allows detailed evaluation of a specific ecosystem and the processes at work there.

2.2.1. SCMs

The idea of a SCM was introduced by Betts and Miller (1986) as a tractable means to evaluate parameterizations developed for General Circulation or Mesoscale models. An SCM runs as a single grid cell, with advective forcing obtained from observations or reanalyses that can be specified in various methods such as

relaxation to an upstream sounding, prescribing advective tendency from observations, or with horizontal advective tendencies coupled with a predicted sounding to prescribe both vertical and horizontal tendencies (Randall & Cripe, 1999). This configuration allows detailed analysis of model performance over a specific domain while constraining computational and storage overhead to easily manageable levels. SCMs have been applied in a number of research applications, from evaluation and testing of cloud parameterization (Cripe & Randall, 2001; Couvreux et al., 2014; Lenderink et al., 2004; Rochetin et al., 2014; Stirling & Stratton, 2012; Sušelj et al., 2012), cumulus parameterization (Aït-Mesbah et al., 2015; Jin et al., 2010; McNider et al., 2012; Sterk et al., 2016; Svensson et al., 2011), and evaluation of surface processes and/or surface-atmosphere interaction (Guichard et al., 2004; Gustafsson et al., 2003; Hu et al., 1999; Stap et al., 2014; Williams et al., 2016).

SCMs have been used to evaluate behavior in tropical South America. The effect of deforestation was studied by da Rocha et al. (1996) who investigated the influence of albedo and surface evapotranspiration on convection for both forested and pasture lands, demonstrating that dry season precipitation can drop over pasture/deforested land when soil moisture drops below a critical threshold. Ganzeveld and Lelieveld (2004) used an SCM in Lagrangian mode to explore the impact of deforestation and moisture on deposition and emission of multiple species. Grabowski et al. (2006) explored boundary layer thickening, cloud formation, and transition from shallow to deep convection in the 6 hr following sunrise for a case taken from the Large-Scale Biosphere-Atmosphere experiment in Brazil. They found that SCMs had a tendency to develop deep convection within 2 hr of sunrise, whereas cloud-resolving models (CRMs) reproduced a more realistic evolution of the boundary layer and transition from shallow to deep convection.

The influences of land characterization on Bowen ratio, ecophysiological stress, and tropospheric dynamics were studied in an SCM application over the KM83 site in the Tapajos River National Forest by Harper et al. (2010; henceforth, HA10). In that study, the land surface model in an SCM was replaced with the land surface characterization described in section 2.1 following Baker et al. (2008). In HA10 simulations of the Bowen ratio were more realistic when compared to eddy covariance observations, planetary boundary layer depth was realistically reduced, and precipitation increased.

2.2.2. Superparameterization

Superparameterization (SP) is the incorporation of a two-dimensional nonhydrostatic CRM within each grid cell of a GCM, sometimes referred to as the multiscale modeling framework (MMF). The CRM replaces the cloud and precipitation parameterizations in the GCM and receives general advective tendencies from the GCM, providing tendencies of moistening and heating in return. Randall et al. (2003) advocate for the use of MMF as a means to "break the cloud parameterization deadlock," meaning that MMF can shed light on a number of cloud-related mechanisms and interactions that have been problematic in climate models for years.

The use of MMFs is becoming widespread and has shown promise in a variety of applications. Simulation of the Madden-Julian Oscillation is improved when MMF models are used (Benedict & Randall, 2009; Pritchard et al., 2014; Thayer-Calder & Randall, 2009; Zhu et al., 2009). The representation of variability in precipitation intensity (DeMott et al., 2007; Kooperman et al., 2016), diurnal variation (Pritchard & Somerville, 2009; Lee et al., 2010), and organized convective systems (Pritchard et al., 2011) is also improved in MMF. MMF applications have also addressed the Indian monsoon (DeMott et al., 2011, 2013) and atmospheric transport of dust and aerosols (Hsieh et al., 2013; Wang et al., 2011).

2.2.3. Land Model: Simple Biosphere Model (SiB)

SiB was introduced (Sellers et al., 1986) as a land surface model for GCMs and was updated to include satellite-derived phenology and coupling of transpiration and carbon processes (Sellers, Randall, et al., 1996) and again with a prognostic canopy air space (Vidale & Stöckli, 2005), new soil and snow treatment, and revised calculation of soil moisture stress (Baker et al., 2003, 2008). SiB has been coupled to GCMs (Randall et al., 1996; Sato et al., 1989; Sellers, Bounoua, et al., 1996) and mesoscale models (Corbin et al., 2010; Denning et al., 2003; Nicholls, 2004; Wang et al., 2007; Schuh et al., 2010), and run in decoupled mode at large scales (Baker et al., 2010; Schaefer et al., 2002, 2004; Zhang et al., 1996), at tower sites (Baker et al., 2003, 2008, 2013; Hanan et al., 2005; Schaefer et al., 2008), in agricultural applications (Corbin et al., 2010; Kim et al., 2001; Lokupitiya et al., 2008, 2016), in model intercomparisons (Lokupitiya et al., 2016; Rutter et al., 2009; Schwalm et al., 2010), and in SCM studies (da Rocha et al., 1996; HA10). SiB has a proven track record of performance. In the experiments presented here, the version of SiB used is identical to that used in Baker

et al. (2008) and HA10. In these simulations leaf area index (LAI) and fraction of photosynthetically active radiation are held constant as in Baker et al. (2008), and the entire grid cell is represented as EBF.

Vegetation as represented by SiB responds to light as shown in Figure 1a, and stomatal conductance and photosynthesis can be downregulated in response to environmental stress. A maximum, or "potential," value for stomatal conductance and GPP is calculated for a given insolation, as shown in Figure 1a, which we refer to as a light response curve. GPP at any given insolation is calculated as the minimum of the rates limited by carboxylation, electron transport, and light response (Collatz et al., 1991, 1992; Farquhar et al., 1980; Sellers et al., 1992). Photosynthetic yield, or the fraction of absorbed photons used for photosynthesis, decreases with increasing light, resulting in a flattening of the curve at high light levels. The light response is further constrained by impediments to plant function in response to low humidity (which is high VPD), low soil moisture, and temperature, shown in Figures 1b–1d. The basic idea is as follows: Photosynthesis is an optimization between the plant's desire to maximize CO_2 uptake while minimizing water loss. Humidity at the leaf surface below the saturated value within the stomate will lead to a closing of stomates as a water-saving mechanism (with attendant reduction in photosynthesis), as will root-zone soil moisture below field capacity (see Baker et al., 2008, for explanation), while temperature will downregulate GPP when canopy temperature falls outside an optimal range, which is specific to vegetation type (Sellers, Tucker, et al., 1996). These mechanisms are calculated as "stress factors," where a value of 1 represents optimal conditions and photosynthesis occurs at the optimal rate, while a value of 0 for any single factor will result in complete closure of stomates. Soil moisture stress is a slow-response function and will vary on time scales of days to weeks or months in response to synoptic- and seasonal-scale wetting and drying cycles. Humidity and temperature will respond to seasonal cycles as well and also on the diurnal scale. These three factors are multiplicative and combined to determine a total stress at every model time step.

For illustration, we have taken the base light response curve shown in Figure 1a (Line 1) and applied a 30% stress to it, or multiplied all GPP values by 0.7 (Curve 2). This may be thought of as indicative of soil moisture stress, which would be almost invariant throughout a single day. In Curve 3 we subject the values of Curve 2 to a further stress at high light values, which may occur due to higher temperatures and/or lower humidity in the heat of the day. We will return to the idea of a light response curve, how stress may change the shape of this curve, and how these responses will influence carbon flux and Bowen ratio throughout this study.

In ecosystems with sparse or moderate canopy coverage, ET will be partitioned into components reflecting transpiration, evaporation of water stored on leaves when precipitation is intercepted before it can reach the ground, evaporation from within near-surface soil, and evaporation from puddles on the ground. In a dense canopy such as at K83 (LAI $\approx$7-m^{-2} leaf per square meter ground), however, the soil components of evaporation are unimportant. Very little direct radiation reaches the soil surface and mixing within the subcanopy air is negligible, so VPD and temperature gradients (and therefore fluxes) at the ground surface are minimal. For this study, the important components of ET (evapotranspiration) are transpiration and evaporation of water off of the canopy.

2.2.4. Model Coupling to Surface

It is axiomatic that the land surface is heterogeneous on the scale of meters. Vegetation, topography, soil moisture, slope, and aspect all vary on scales much smaller than all but the most highly resolved models. Wind and surface/subsurface drainage can partition the landscape into dry uplands and moist riparian areas, and transient convective precipitation can moisten a subset of the landscape across both upland and riparian regimes.

The nonlinear processes shown in Figure 1 impose a strong constraint on stomatal conductance (and therefore GPP), transpiration, and Bowen ratio. Soil moisture stress (Figure 1b) is almost invariant as soil moisture decreases initially from field capacity but has been observed to drop steeply once a threshold, dependent upon vegetation and soil type, has been encountered (Colello et al., 1998; Entekhabi & Eagleson, 1989; Laio et al., 2001; Muchow & Sinclair, 1991). Photosynthesis increases linearly with increasing light at low illumination, but saturates with higher insolation (Jarvis, 1976; Miranda et al., 2005; Figure 1a).

Nevertheless, most models currently used today, especially GCMs, incorporate a single value to represent surface-atmosphere interaction. Simulated air and canopy temperature, soil moisture, and water vapor mixing ratio all represent mean values across the landscape, on the scale of 100 km or more. If the physical processes that control surface-atmosphere exchange were linear, this mean value would be appropriate. But the fact that we are calculating nonlinear relationships using a mean value sets up a version of Jensen's

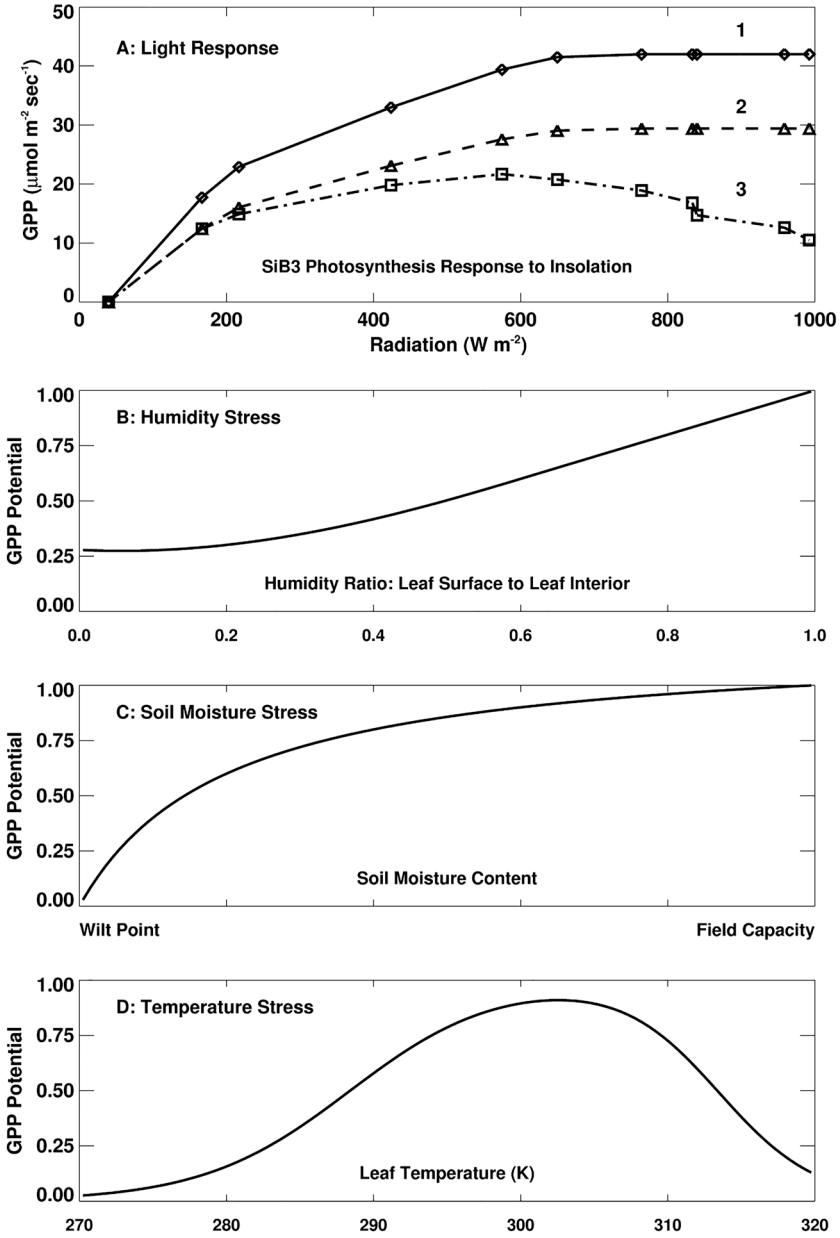

Figure 1. Example of SiB3 GPP response to radiation, or light response curve (a). Simulation results are taken from Baker et al. (2013), and some values have been slightly altered for presentation smoothness. See text for explanations of Curves 1, 2, and 3. (b–d) Model constraint on potential GPP via stress from low humidity across the stomate, soil moisture deficit, or hot/cold temperature. GPP = gross primary productivity; SiB3 = Simple Biosphere Model Version 3.

inequalty (Jensen, 1906), or

$$F(\bar{x}) \neq \overline{F(x)}. \tag{1}$$

Conceptually, we can envision that the mean of spatially heterogeneous nonlinear influences on evapotranspiration and photosynthesis may not be equal to the calculation of these processes using a domain-averaged input value. While MMF may be seen as a remedy to this issue, most first-generation MMF models such as the superparameterized (SP) Community Earth System Model (Khairoutdinov & Randall, 2001; Khairoutdinov et al., 2005) take the average of quantities such as precipitation, temperature, wind, and humidity as they come out of the CRM elements and pass a domain-mean value into a *single land surface model*. In this case the high-resolution and potentially heterogeneous forcing generated by the CRMs is averaged back to

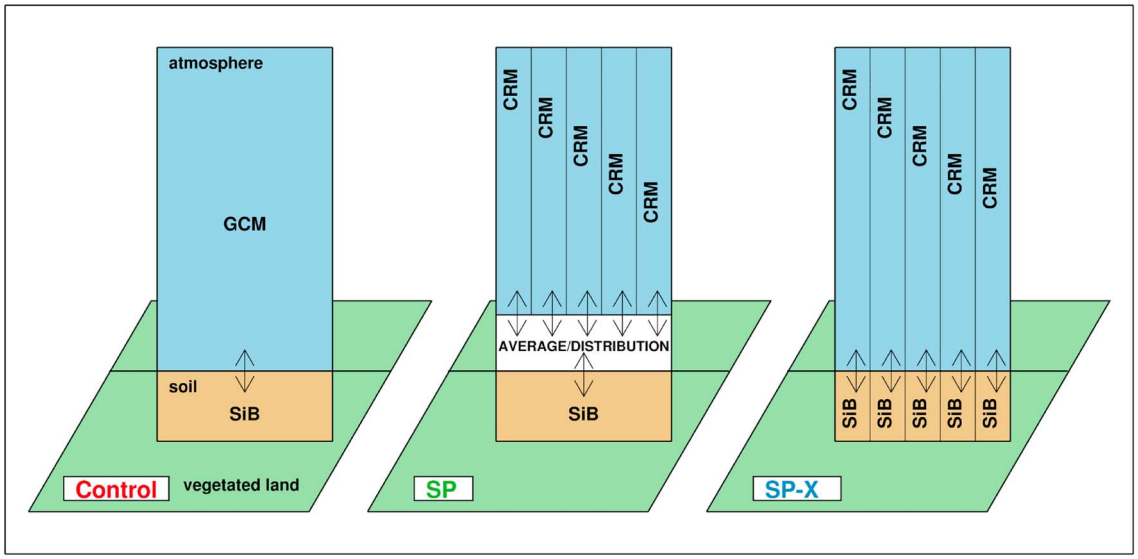

Figure 2. Schematic showing surface-atmosphere coupling for traditional GCM (Control), first-generation MMF models (SP), and an MMF model with each CRM element coupled to its own land module (SP-X). CRM = cloud-resolving model; GCM = General Circulation Model; MMF = multiscale modeling framework; SiB = Simple Biosphere Model; SP = superparameterization; SP-X = superparameterization with highly resolved surface coupling.

a GCM grid cell mean value used for calculation of surface fluxes, and the problem of Jensen's inequality remains.

2.2.5. Experimental Setup

In this experiment, we evaluate the surface-atmosphere interaction at the K83 site employing three model configurations, shown in Figure 2, all in the SCM framework. The first is traditional GCM physics using cloud parameterizations as in HA10 and a single representation of the surface. We call this configuration the *Control*, and it represents the canonical treatment in GCMs. The second model replaces cloud and precipitation processes in a first-generation MMF configuration with CRM-mean forcing applied to the surface, as in SP-Community Earth System Model. This configuration is referred to as *SP*. Finally, we have constructed a model similar to SP, except that each CRM element is coupled to its own surface model. These explicitly resolved surfaces allow independent evolution of soil moisture and associated influence on canopy processes, temperature, humidity, and carbon cycle (GPP and respiration), as well as the influence of heterogeneous surface flux back into each element of the CRM. There is no heterogeneity in the surface vegetation or soil type; each CRM is coupled to a land surface specified as EBF (tropical forest). We call this model configuration *SP-X, or SP with extra coupling to the surface*. Both SP and SP-X are MMFs, and SP-X couples to the land surface at high resolution, while SP couples to the land surface on the scale of the GCM grid cell.

The CRM used here is based on the large-eddy simulation model of Khairoutdinov and Kogan (1999), later modified for coupling to the National Center for Atmospheric Research Community Climate System Model (Khairoutdinov & Randall, 2001) global simulations and comparison to Atmospheric Radiation Measurement Program Southern Great Plains observations (Khairoutdinov et al., 2005). Moist convection and large-scale condensation (stratiform) parameterizations are replaced with explicit representations of these processes, although parameterizations around hydrometeor size and concentration remain in cloud microphysics calculations. Longwave and shortwave radiative flux calculations are based on the Rapid, accurate Radiative Transfer Model (RRTM; Clough et al., 2005; Iacono et al., 2000; Mlawer et al., 1997), but global cloud fraction is explicitly calculated rather than parameterized. Following Khairoutdinov and Randall (2001) there are 64 CRM elements in each grid cell and the CRM is incorporated as a two-dimensional "curtain" oriented in an east-west direction. Each CRM element has a spatial domain of 2 km each, which maps to an approximately 1° grid cell size with the 64 elements. Surface heterogeneity is not represented; all instances of land in Control, SP, or SP-X are treated as EBF. Lateral boundary conditions are cyclic.

Each model is forced with National Center for Environmental Prediction (NCEP) reanalysis (Kalnay et al., 1996), as in HA10. That paper demonstrated that an improved land surface model, following Baker et al. (2008), resulted in more realistic simulation of surface fluxes and atmospheric behavior. We use HA10 as

the Control here. In this experiment we will be evaluating the change in behavior when parameterized clouds and convection are replaced with a CRM (Control to SP/SP-X) and also the change in behavior when coupling scale at the surface is decreased from order 100 km to order 4 km (SP to SP-X). All models are simulated for the period 2001–2003 as in HA10, and all models are spun up by repeating the 3-year forcing for five cycles, or 15 years prior to analysis.

In this manuscript we consider a number of questions pertaining to the fate of water as represented in the three model configurations:

- What is the intensity of precipitation that falls on the forest?
- Does the precipitation intensity facilitate evaporation of water off of leaves, as opposed to rainfall exceeding leaf storage capacity and reaching the ground?
- How is water stored in the soil in the wet season and used during the dry season?
- How is land-atmosphere exchange affected by coupling scale and precipitation dynamics?

Ultimately, we are interested in how model configuration, in the formulation of cloud, precipitation, and radiation parameterizations, combined with the scale of land-atmosphere coupling, influences the representation of these processes and the ultimate path a water molecule makes during its journey from hydrometeor through being locally lost via runoff or ET. In this experiment we will, through evaluation against available observations, identity the mechanisms and processes that control the fate of water *for this location and perhaps others that occupy the same location in vegetation and climate space as represented by total precipitation and length of dry season*. Although we cannot extrapolate our findings to the entire basin, our analysis may provide a framework useful for investigations of MMF- versus traditional GCMs in regional or global applications.

3. Results and Discussion

In this section we extend the body of work that begins with Baker et al. (2008) and HA10. Baker et al. (2008) demonstrated that simulated vegetation behavior and land-atmosphere flux could be made consistent with observations, and HA10 showed how atmospheric behavior was altered in an SCM by changing *only* the surface module. Here, the land module (Baker et al., 2008) is consistent between all models; What is changed is the atmospheric representation, from the Control configuration (HA10) to an MMF configuration with aggregated land (SP) to a model where each CRM element is coupled to its own land model on scales much smaller than for Control or SP. We confront results from the three simulations with observations as an evaluation tool. We begin with precipitation, as this is the primary driver of ecophysiological function in this region. We next look at radiation and Bowen ratio components (LE and H) as more traditional forms of evaluation. Finally we investigate the "fate" of water as it moves from hydrometeor through the soil-plant system and the carbon-climate interactions.

3.1. Precipitation

Monthly averaged precipitation, standard deviation, and fraction of hours with rain from all three models as well as observations are shown in Figure 3. At the K83 site the wet season runs from approximately January through June. During the period of observation (2001–2003) the dry season (July–December) can be extremely dry, as in 2002, relatively wet (2003), or intermediate (2001). The observed precipitation spike (and attendant large standard deviation) in November 2002 results from a single large event observed at the K83 tower. All three models simulate monthly mean precipitation values very similar to observations with respect to timing of wet season and amplitude of monthly mean (Figure 3a). This is not surprising, as NCEP reanalysis is forcing the large-scale tendencies in all three models, so observed overall trends in moisture divergence must be reproduced in accordance with reanalyses. However, the variability and frequency of precipitation are quite different. Control precipitation shows little or no variability: Rain intensity is almost constant (Figure 3b). The multiscale simulations (SP and SP-X) have increased variability but only approach the observed value during the dry season. Consistently, the fraction of time with precipitation occurring (Figure 3c) reflects these points: The Control is producing rain almost all the time, even in the dry season. The multiscale runs (SP and SP-X) approach observed precipitation frequency in the dry season, but wet season rainfall occurs as more frequent events with less intense rainfall than the observed infrequent heavy rain.

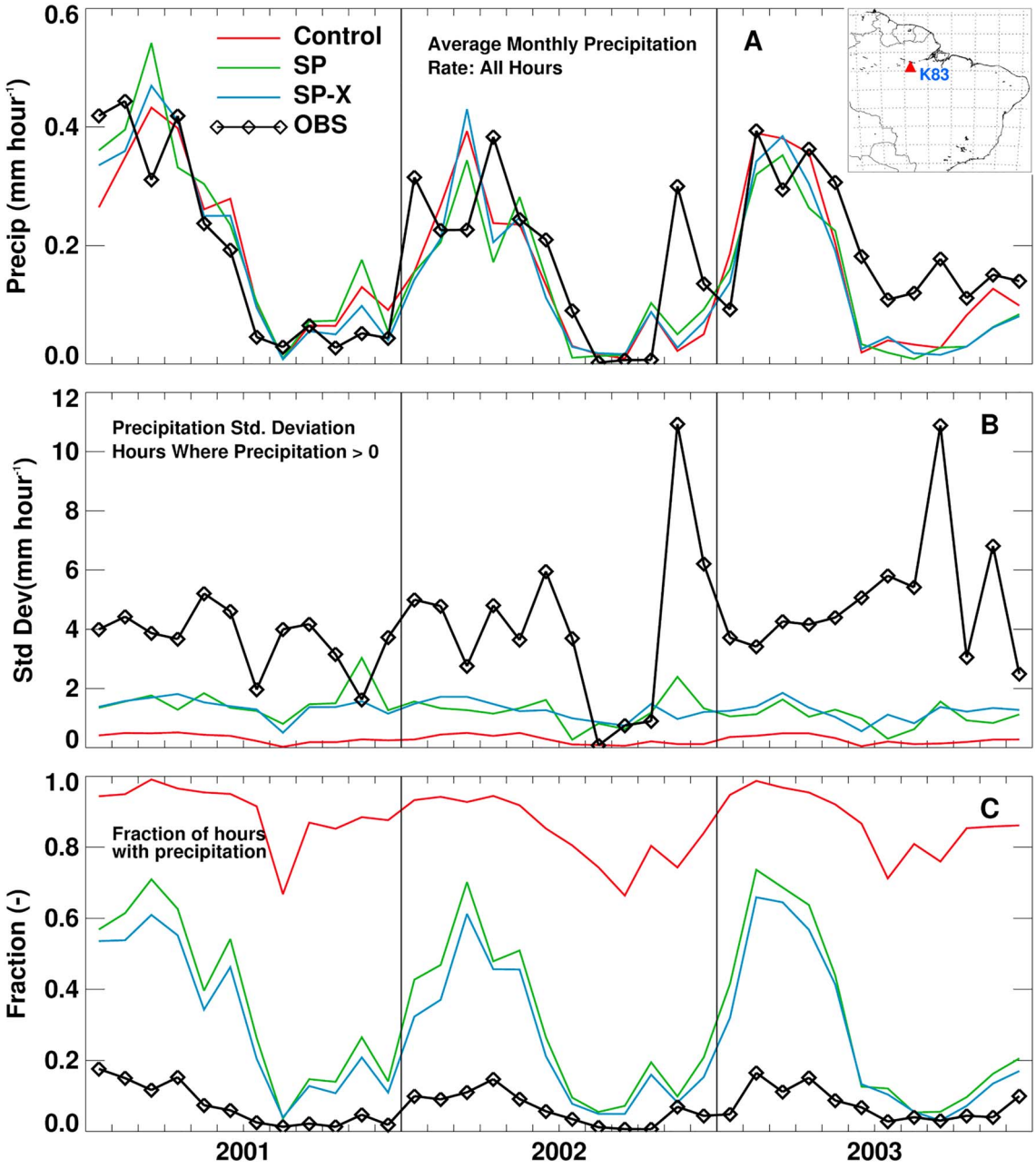

Figure 3. (a) Monthly mean precipitation as observed at the K83 site for 2001–2003 and as simulated by the three models. (b) Standard deviation in precipitation, for those hours where precipitation is nonzero. (c) Fraction of hours in the month that report rain. Inset in (a) shows site location. SP = superparameterization; SP-X = superparameterization with highly resolved surface coupling.

These results are similar to those found by DeMott et al. (2007), in that a traditional GCM (similar to Control) underrepresented the contribution of intense rainfall events in the Amazon basin. However, DeMott et al. (2007) also found that their multiscale model (MMF, analogous to SP) almost exactly reproduced the occurrence and contribution of the most intense precipitation events and underrepresented light and intermediate rain events (10 to 20 mm/day). It bears noting that DeMott et al. (2007) were comparing a free-running GCM simulation to Global Precipitation Climatology Project data (Version 2; Huffman et al., 2009) over a much larger region. In our case, our observations are from a single tower site where the models are forced by reanalyses, so the comparison is not identical.

The "perpetual drizzle" in the Control will have consequences for simulations of ET and its partitioning. Leaves will capture and store this light rainfall, and evaporation of this reservoir can compose a

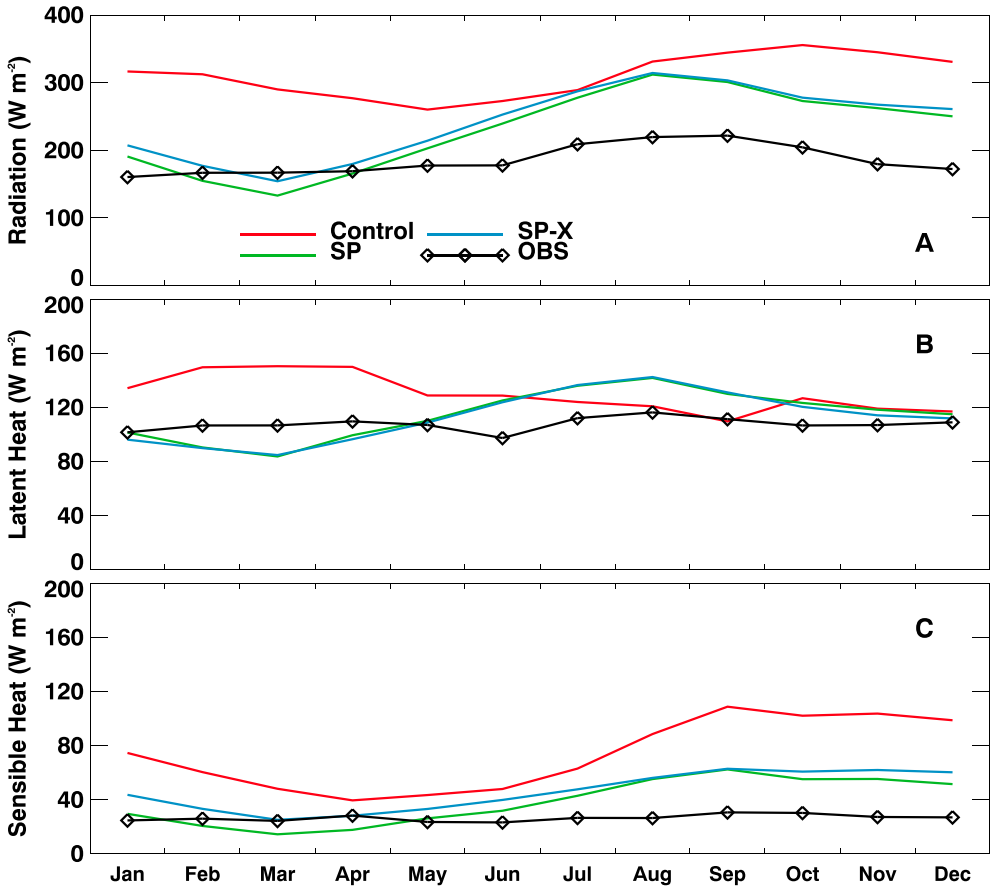

Figure 4. Average annual cycle (2001–2003) of incoming shortwave radiation (all hours) as observed at the K83 tower and for all three models (a). Mean annual cycle for latent heat is shown in (b), and sensible heat is shown in (c). SP = superparameterization; SP-X = superparameterization with highly resolved surface coupling.

significant fraction of total latent heat flux. This canopy interception problem is not new; Shuttleworth (1988a) described it as a pathway for unrealistically large (or small) evaporation. Eltahir and Bras (1993a) demonstrated that total ET can be overestimated with unrealistic canopy interception, although their study emphasized the parameterization of water amount stored on leaves, as did Dolman and Gregory (1992), as opposed to rainfall intensity. We will return to this topic in section 3.4.

3.2. Radiation

Modeled radiation is compared to observed in Figure 4a. Observations are taken from the gap-filled product of de Gonçalves et al. (2013). The multiscale models (SP and SP-X) use RRTM radiation, with cloud fraction calculated explicitly. Control radiation follows Stephens et al. (2001) and exceeds observed in all months. This difference is attenuated by nighttime hours, which is approximately half the hours since this is a tropical site (3°S latitude). Therefore, at midday, Control insolation can exceed observed by 300 W/m^2 or more in the mean. The amplitude of the seasonal cycle in the Control has similar amplitude to observed, but the month of peak radiation lags observed by 1–3 months. The amplitude of the SP/SP-X insolation cycle is larger than observed and slightly larger in the mean. During March SP/SP-X radiation is less than observed and exceeds observed in other months. The annual cycle of the multiscale models is in phase with observations.

The distribution of daytime (1000–1600 LST) insolation into radiation bins for March, a wet month, is shown in Figure 5. Here, we take observations from Restrepo-Coupe et al. (2013) so as not to bias the distribution with gap-filled hours. The observed radiation probability density function (PDF; top left) is almost flat below 750 W/m^2 and over 85% of the observations fall in this range. The Control radiation PDF does have some density in the low end but less than 50% of observations are below 750 W/m^2, and peak density is in the range 900–1,050 W/m^2 where fewer than 10% of observations occur. SP-X (bottom right) has a PDF very similar to observed; all bins between 0 and 750 W/m^2 have between 15% and 20% density, with no distinct

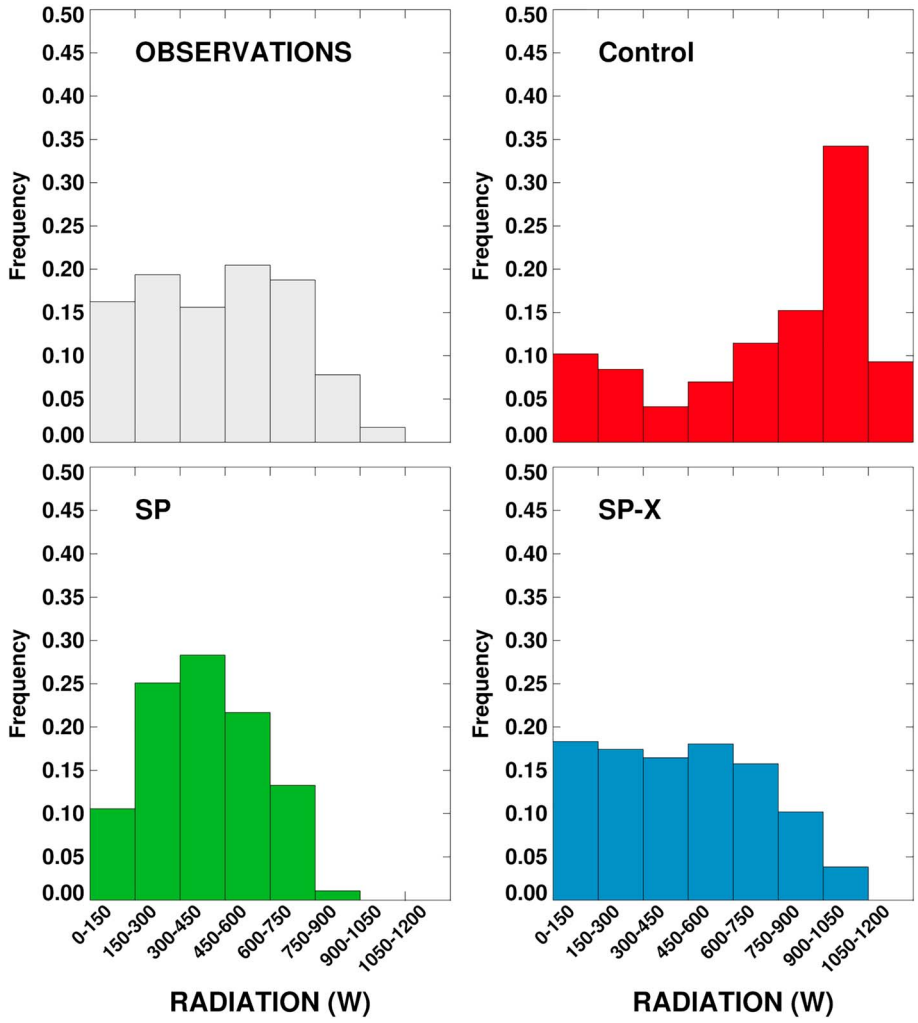

Figure 5. March distribution of incoming shortwave radiation, for hours 1000–1600 local time, as observed at the K83 tower and for all three models. SP = superparameterization; SP-X = superparameterization with highly resolved surface coupling.

peak, and accumulated density below 750 W/m^2 is >85% of the total. SP, which averages cloudy and clear CRMs to obtain a single radiation value which is passed to the surface, is more peaked in the middle. One can envision the SP distribution being "squeezed" from each end, as very bright and dim CRM radiation values are averaged into a single value before being passed to the land module.

The distribution of daytime radiation for September is shown in Figure 6. Observed radiation PDF (top left) now has a peak in the 600–750 W/m^2 range and lower occurrence in the darkest bins, although there is nonzero area there. There is <25% area in bins where radiation >750 W/m^2. Control radiation is again very high when compared to observations, with over half of midday insolation values higher than 900 W/m^2. SP-X peaks in the 900–1,050 W/m^2 bin (as do Control and SP) and has less density than observed in the lowest bins. SP shows the characteristic tendency, when compared to SP-X, of having area squeezed from the lowest and highest bins toward the middle, a consequence of averaging.

3.3. Surface Moisture and Energy Flux

The average annual cycle (2001–2003) of latent and sensible heat (LE and H, respectively) is shown in Figures 4b and 4c. Observed LE and H are almost invariant through the year, although LE rises slightly at the onset of the dry season. Simulated annual cycles of LE and H show much more amplitude. The Control is larger than observed, for both LE and H, for almost all months of the mean annual cycle. Control fluxes are quite seasonal, showing a peak-to-peak amplitude of ~40 W/m^2 in LE and ~70 W/m^2 in H, with LE minimum/H maximum in the dry season. Fluxes from the multiscale models (SP and SP-X) are much

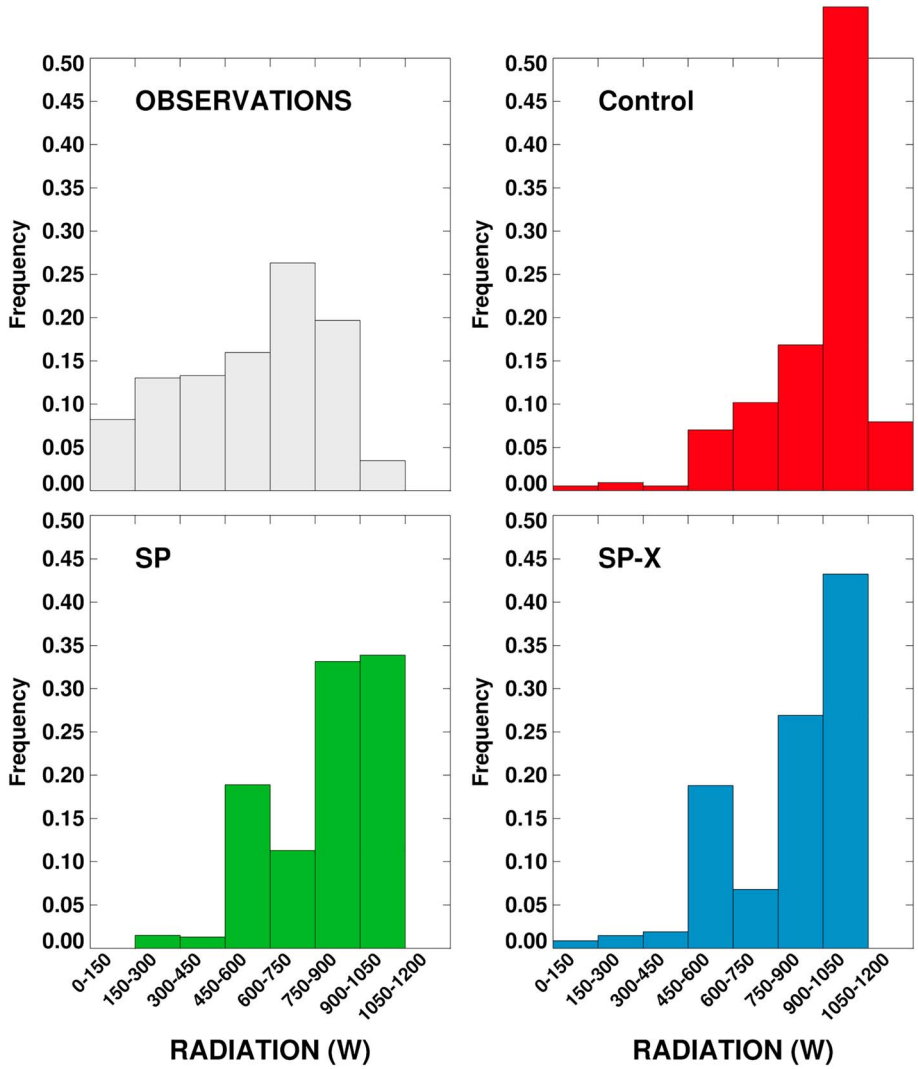

Figure 6. Similar to Figure 5 but for September.

closer to observations. Both SP and SP-X have an increase in H during the dry season, but LE peaks during the dry season as well, so Bowen ratio is relatively unchanged during the year, resembling observations (not shown). The large insolation of the Control must be balanced by soil heat flux, canopy heat storage, and LE and H. As the albedo calculation is identical between the three models, and soil heat flux is small due to the dense canopy, it is inevitable that LE and H calculated by the Control will be larger than that of SP and SP-X.

3.4. The Fate of Water

Water that precipitates out of clouds can return to the atmosphere via transpiration through stomates, evaporation off leaf surfaces, from the surface soil or from puddles that form on the ground; it can be stored in the soil or lost as surface and subsurface runoff. The tendency of traditional models (Control) to generate long-lived light precipitation when compared to more realistic intensity distributions in MMF models has been noted previously (DeMott et al., 2007; Kooperman et al., 2016). In the EBF at K83, heavy rain quickly exceeds canopy capacity to store water, resulting in increased water reaching the soil surface where it can infiltrate or run off. Constant light rain in the model can result in unrealistically large ET as water is recycled to the atmosphere quickly without going through storage in soil (Davies-Barnard et al., 2014; Dolman & Gregory, 1992; Eltahir & Bras, 1993b; Pitman et al., 1990; Shuttleworth, 1988b), although excessive canopy evaporation in models can also result from unrealistically large storage capability on leaves (Davies-Barnard et al., 2014; Eltahir & Bras, 1993a). Unrealistic canopy evaporation can also influence the timing of seasonal cycles, as water storage in soil will impose a time lag between precipitation and water release. Recall from

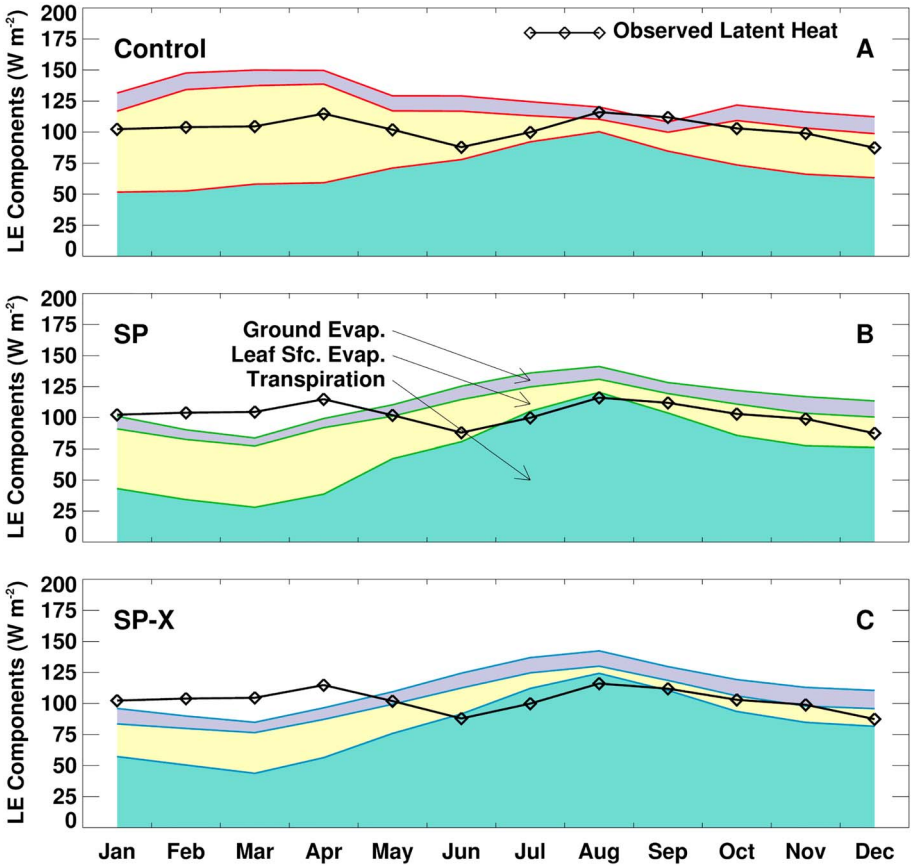

Figure 7. Mean monthly partition of evapotranspiration into evaporation out of the soil, evaporation off of leaf surfaces, and transpiration for all three models. Observed evapotranspiration is shown as a black line. LE = latent heat; SP = superparameterization; SP-X = superparameterization with highly resolved surface coupling.

Figure 3 that the Control has almost constant light rain, while the CRMs in the multiscale models result in a larger standard deviation and lower frequency of rain that indicates a higher frequency of heavy precipitation events. SP will have a lower incidence of the highest-intensity precipitation events than SP-X will, as CRM elements with heavy precipitation will be averaged together with nonprecipitating CRM elements during SP averaging.

Therefore, we might expect evaporation of water from leaves to decrease from the Control to SP to SP-X, and this is in fact seen in Figure 7. During the wet season, canopy evaporation can equal or exceed transpiration in Control and SP, but transpiration is the largest contributor to overall ET in SP-X during the entire year. This behavior is directly linked to precipitation intensity. The almost continuous "drizzle" in the Control results in leaves that are consistently wet, as well as a canopy interception storage amount that frequently does not exceed the limit as specified in the model. In SP-X, brief, intense rainfall events exceed canopy storage limits resulting in water reaching the ground where it can run off or infiltrate to be returned to the atmosphere later as transpiration. In SP, light and intense rainfall events are "smoothed out" during the averaging process, and a single precipitating CRM element results in a reduction in the number of events where canopy storage capability is exceeded and an increase in wet canopy incidents that suppress transpiration. The precipitation intensity acts as an influence on canopy interception efficiency.

Near-instantaneous canopy behavior during a single day in March (wet season) is shown in Figure 8, for the morning (a and c) and afternoon (b and d). There are large dots representing Control and SP; individual SP-X CRM element behavior is shown as small dots, and the SP-X grid cell mean is the large blue dot. In the morning (a) Control radiation exceeds both SP and SP-X, which are similar. GPP is largest in SP, reflecting the fact that "dark" CRMs are averaged in with "bright" ones, with the net result being a shift of the mean up the light response curve (cf. with Figure 1). The fact that Control GPP is less than SP, even

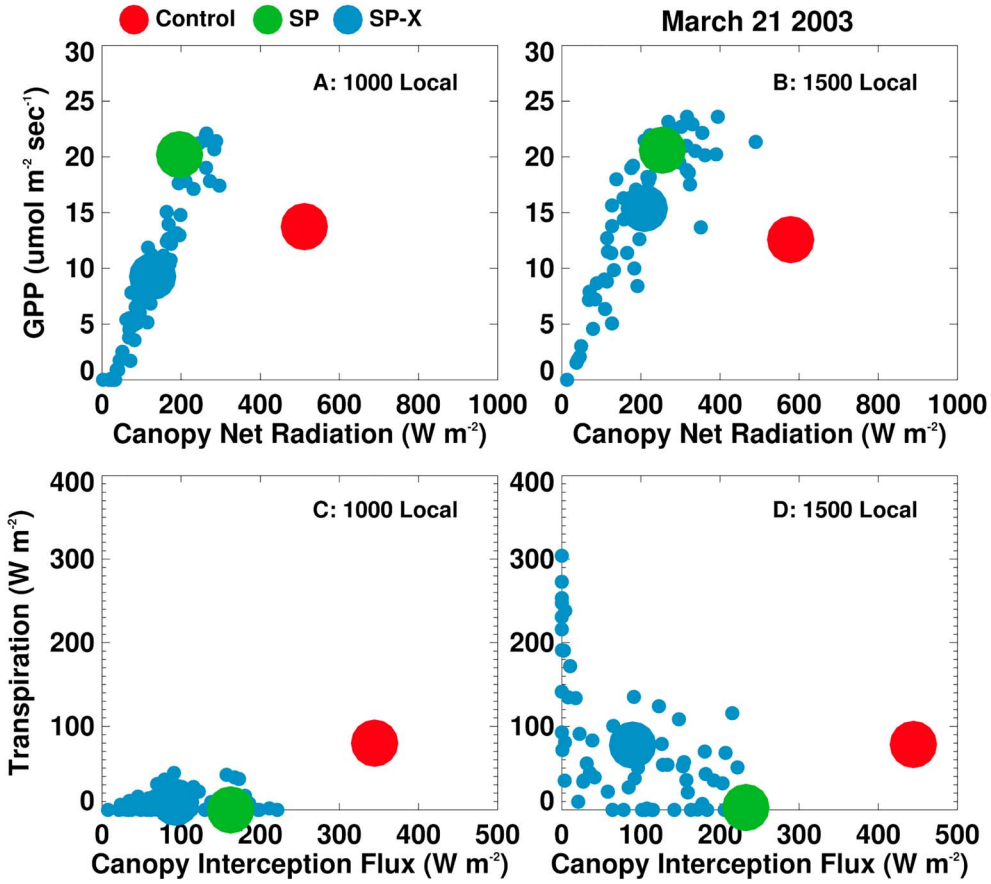

Figure 8. "Snapshots" of GPP versus radiation and transpiration versus evaporation of water off of leaves (Interception flux) at 1000 and 1500 local on 21 March 2003. GPP = gross primary productivity; SP = superparameterization; SP-X = superparameterization with highly resolved surface coupling.

with higher light levels, suggests that water limitation or other canopy stress exists in the Control even during the wet season. In SP-X, mean GPP is less than either Control or SP due to the presence of some CRM elements with dense clouds and low radiation. In the afternoon (b) Control GPP is slightly less than it was in the morning, even at higher light levels, which is an indication of increased stress since the morning due to high temperature and/or high VPD. Under these stressed conditions, the canopy cannot cool itself sufficiently with transpiration, resulting in hot leaves and further stress and stomatal closure. SP GPP is almost unchanged from the morning, but SP-X GPP has increased due to higher overall light levels and fewer very dark CRMs. The SP-X CRM elements reveal a shape that looks very much like a light response curve. However, the range of CRM GPP from 13–23 $\mu mol \cdot m^{-2} \cdot s^{-1}$ at an illumination of ~400 W/m^2 indicates that some CRM elements are unstressed, while others may be experiencing reduction in GPP due to increased temperature or VPD. This heterogeneity arises as a function of the smaller coupling scale in SP-X.

The relative contributions of canopy evaporation (X axis) and transpiration (Y axis) to total latent heat flux are shown in the bottom two panels. In SiB, a fully wet canopy has no transpiration, and canopy fractional wetness is a function of LAI and amount of water stored on leaves. In the morning (a), SP has no transpiration, demonstrating that 100% of the canopy is wet and all LE comes from evaporating water stored on leaves. In the Control, canopy evaporation is greater, but transpiration is nonzero; this indicates that the canopy has fractional wetness, but the higher insolation results in greater overall canopy ET. SP-X has many fully wet CRMs (no transpiration) and many partially wet CRMs that will have nonzero transpiration and canopy evaporation. The CRM elements with near-zero transpiration and interception flux are very dark due to clouds. In the afternoon, Control transpiration is unchanged, but canopy evaporation has increased in response to higher light levels (d). This underscores the Control's tendency to simulate almost continuous precipitation while maintaining unrealistically high insolation. In SP, the canopy is still completely wet,

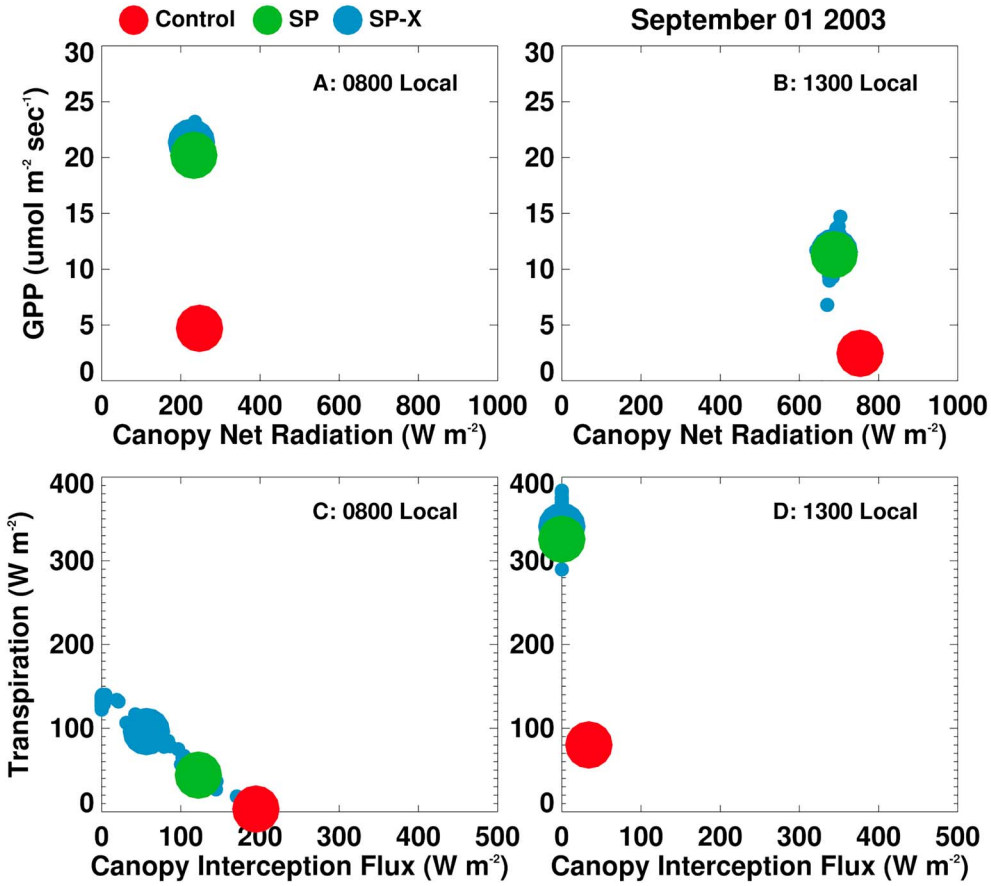

Figure 9. Similar to Figure 8 but for 0800 and 1300 local time on 1 September 2003.

due to the averaging of CRM behavior. A few precipitating CRM elements provide enough rain to keep the canopy wet. In SP-X, individual CRM elements display a range of behavior. Some elements have completely wet leaves; these are the points that lie along the X axis, and varying light levels drive interception flux values from 0 to 250 W/m^2. Some CRM elements are completely dry; these lie along the Y axis, again with varying amounts of transpiration. Some SP-X CRM elements are partially wet, and these are the points that have nonzero transpiration and canopy evaporation fluxes.

Dry season behavior during a single day (1 September 2003), similar to Figure 8, is shown in Figure 9. In this figure 0800 and 1300 local time are shown in (a) and (c), and (b) and (d), respectively. Radiation is similar for all three models (a and b) during both morning and afternoon hours, due to reduced cloudiness in the dry season. All three models also indicate temperature and/or humidity stress, as afternoon GPP values are lower in all models. Soil moisture stress does not change appreciably during the course of one day. Hot dry weather results in increased canopy temperature and VPD. In the morning, leaves are at least partially wet in all three models (c), resulting in nonzero interception flux. The morning canopy wetness can result from either precipitation or dewfall. The canopy in the Control is completely wet (no transpiration), while SP and SP-X are partially dry (both transpiration and canopy interception flux nonzero). The CRM elements in SP-X partition transpiration and canopy evaporation linearly from completely wet (zero transpiration) to completely dry (zero canopy interception flux). This suggests that there are few clouds and no precipitation, and CRMs are evaporating dew heterogeneously in response to variable light levels. In the afternoon, the canopies in both SP and SP-X are completely dry. There is very little heterogeneity in individual SP-X CRM elements on this particular day, indicating almost uniform lack of cloudiness and/or rain. In the Control canopy interception flux is nonzero, which is indicative of continuing light rain, even in the dry season.

It is important to recognize that these three models will not respond identically to the tendencies applied to force the CRM. General tendencies of precipitation in wet and dry seasons are consistent between the models (Figure 3), but individual days are not guaranteed to have the same weather. The Control tendency

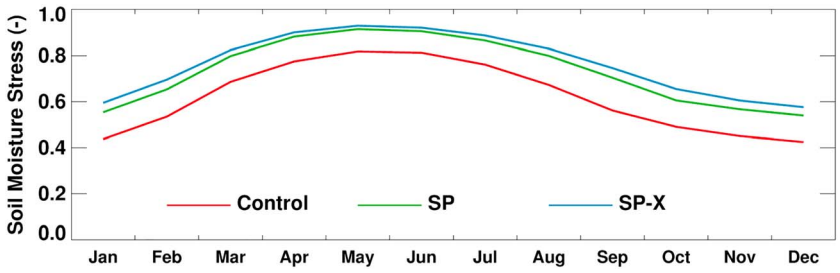

Figure 10. Mean annual cycle of soil moisture stress for all three models. A value of 1 indicates no stress; a value of 0 will result in completely closed stomates. SP = superparameterization; SP-X = superparameterization with highly resolved surface coupling.

for near-continuous light precipitation is conspicuous in both these two samples and many other days. The radiation scheme used in the Control (Stephens et al., 2001) produces insolation similar to RRTM for the dry season day shown here but has much higher radiation on the average in all months (Figure 4).

The fate of water, as expressed in the three models, has a significant effect on water storage in the soil. Soil moisture stress is a nonlinear constraint on stomatal conductance (Figure 1c), transpiration and GPP (Baker et al., 2008). The mean annual cycle of this stress factor is shown in Figure 10. This stress factor in the Control is smaller (more stress) than for SP or SP-X for the entire year; this is a direct consequence of light precipitation, resulting in evaporation of water off of leaves at the expense of water availability for infiltration and storage in the soil. Furthermore, the higher insolation in the Control during the entire year has the effect of generating a large evaporative demand during all months (Figures 4 and 7), so that during the wet season there is not enough storage increase in the soil to bring the soil moisture stress factor back to a value of 1, or unstressed. Both SP and SP-X have soil moisture stress factors ~0.2 higher than the Control, with this offset slightly less at the end of the wet season in May. This is attributable to the combination of higher precipitation variability, as well as more realistic (less) insolation. SP soil moisture stress is slightly more (lower value) than SP-X due to the averaging of CRM output to force the land surface module, which results in fewer extremely intense precipitation events that exceed leaf water storage capacity.

3.5. Carbon-Water Linkage

The hydrological and carbon cycles are linked through stomates; in this region, where LAI is large and evaporation of water directly out of the soil is small (Figure 7), this coupling is particularly tight. We represent this linkage in Figure 11, where radiation during the hours 1000–1600 local time (for all days in the month, 3 years of simulation) is binned in 150-W/m^2 increments on the X axis (as in Figures 6 and 7) and GPP, as calculated for the K83 site by Restrepo-Coupe et al. (2013) and from the models, is shown on the Y axis. Symbol size is scaled by the relative fraction of occurrence in each bin, with larger circles representing a higher density of points falling within that particular bin. Observational and model data are hourly, although SP-X will have 64 CRM values at each hour where observations and Control/SP have only one.

March is one of the wettest months of the year (Figure 3). The observation curve very strongly resembles a light response curve with little or no stress in that GPP increases with increasing light at low insolation and the response is attenuated at higher light levels (cf. to Figure 1). There is not a decrease in GPP with increasing light at the highest radiation levels, indicating that neither high temperature and/nor VPD was acting to impose stomatal closure under the brightest daytime conditions. This is consistent with a wet month where water limitation is not an issue. The Control behavior is inconsistent with this. Soil moisture stress in the Control is around 0.5 (Figure 10) in February, which will restrict GPP potential as partially closed stomates across all radiation levels. At the higher radiation values in the Control (above 600 W/m^2), GPP does decrease slightly with increasing radiation, suggesting temperature or VPD stress is a factor during these bright periods. Transpiration cannot keep up with evaporative demand, resulting in warmer and drier canopy air. The Control radiation distribution (when compared with observations; see Figure 6) is skewed too large. SP has the least response in GPP with changing canopy illumination, which is consistent with the CRM averaging pushing insolation at the surface toward intermediate values. SP-X more closely resembles the observed distribution of GPP versus radiation. SP has higher GPP than observed at low light levels and lower GPP than observed at high light levels, while SP-X is biased slightly low (at all radiation levels) when

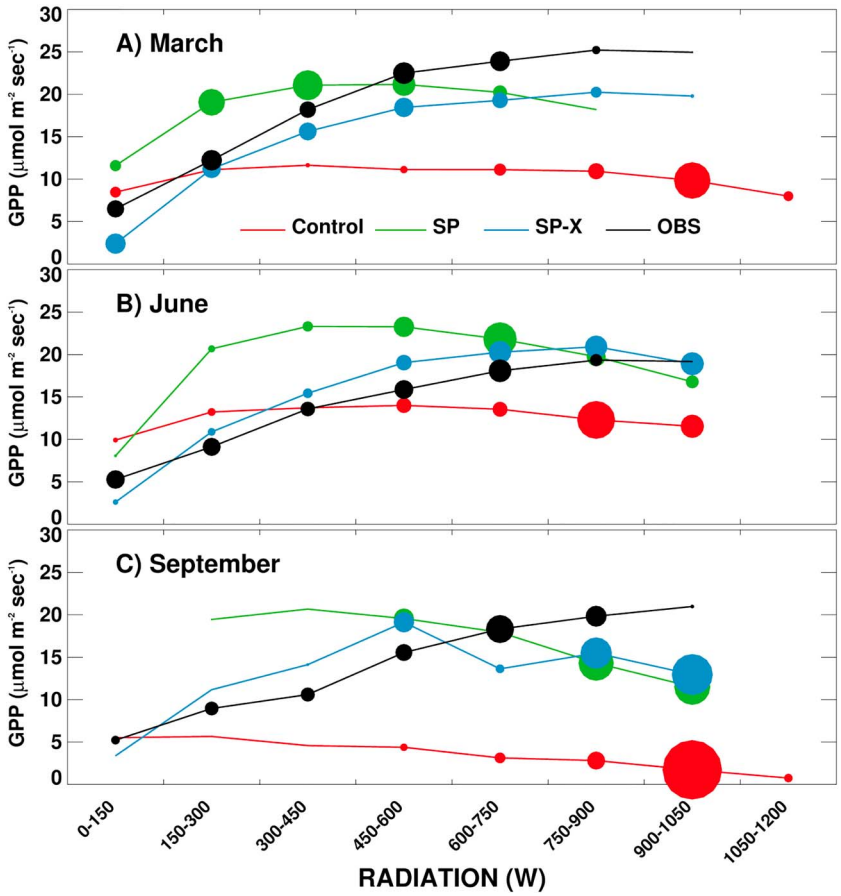

Figure 11. Radiation-GPP curves for hours 1000–1600 for all three models and observations for the months of March, June, and September. Size of dots represents frequency of occurrence in a particular radiation bin, compare with Figures 5 and 6. GPP = gross primary productivity; SP = superparameterization; SP-X = superparameterization with highly resolved surface coupling.

compared to observations. Similarly, the SP-X radiation distribution most closely resembles observed (see also Figure 5).

June marks the transition between wet and dry seasons. The observed GPP response to increasing light retains the shape of a light response curve, shifted downward slightly from February values. Soil moisture stress in all models (Figure 10) is near the peak value (lower stress), as a result of higher precipitation exceeding ET during the wet season and building up water storage. All models, for all radiation bins, are at or near peak GPP in June. The Control GPP response to increasing light on the diurnal scale, while shifted upward from February, still appears similar to a stressed light response curve (i.e., Curve 3 in Figure 1a). GPP is relatively flat with increasing radiation, due to stress caused by low humidity at the leaf surface at higher light levels. Both SP and SP-X look like light response curves, and both do show some decrease in GPP at higher light levels, due to leaf surface humidity stress. The SP-X curve follows the observations very closely, but has a higher number of low-radiation events.

By September, all models are experiencing some level of stress, yet the observations still show increase in GPP with insolation. Figure 11 shows that the vegetation in the Control is under strain; GPP levels are all low and decrease with brightness. SP and SP-X both experience leaf surface VPD stress at light levels above 300 W/m^2, and high temperature stress above 600 W/m^2.

An interesting feature of Figure 11 is that SP has higher GPP within a given light "bin" at lower insolation, and lower GPP in the highest bins, when compared to SP-X. There are several reasons for this. The lowest two bins (0–300 W/m^2) are in the region where photosynthesis is extremely responsive to light. The averaging across CRM elements in SP results in fewer points in these lower bins (note size of the dots in Figure 11),

and the mean value within the bin to be higher. At very low light levels it is possible for simulated GPP to be smaller than the dark respiration calculated in SiB (Collatz et al., 1991; Farquhar et al., 1980), resulting in zero gross uptake. In SiB, for the canopy represented at K83, this happens at insolation below approximately 40 W/m^2, although it can happen at higher insolation if stress is being imposed on photosynthesis. In SP, these events are almost entirely smoothed out by the averaging across CRMs, with the net result that SP GPP is much higher than SP-X (or observed) in the lowest bin. In other low-radiation bins, there can be higher stress (usually low leaf surface humidity) in individual CRMs in SP-X, dropping the GPP to slightly lower levels than SP. In the very brightest radiation bins, the situation is reversed, and SP has more leaf surface VPD stress than SP-X.

In the observations, maximum GPP occurs in February and March, in the wet season, while in the models maximum GPP is from April to July, or during the period immediately after seasonal rains have diminished in intensity and frequency. Minimum observed GPP is during August, while all models minimize GPP at the end of the dry season (November–December) due to depletion of stored water in the soil. Wu et al. (2017) and Restrepo-Coupe et al. (2017) discuss a partial litterfall at the end of the wet season and relatively rapid regrowth following. The new leaves, however, have low photosynthetic capacity for 30–60 days following flush. These processes may influence the observed GPP seasonality (which is still relatively low), yet SiB does not currently allow for changing photosynthetic capacity during the year and therefore cannot reproduce this mechanism.

The SP-X curve follows the observed closely in all months, not just those shown. While this is encouraging, it is not a confirmation of SP-X realism or performance (e.g., Franks et al., 1997; Keenan et al., 2011). Equifinality, or the ability to "get the right answer for the wrong reason," is a possibility; furthermore, the methods used to partition observed net CO_2 flux into photosynthetic and respiratory components are not uniform (Lasslop et al., 2010; Falge et al., 2002; Reichstein et al., 2005; Valentini et al., 2000) and can be subject to challenge (Reichstein et al., 2005; Wohlfahrt & Galvagno, 2017), casting some doubt on the veracity of "observed" GPP. However, the SP-X simulations are some of the closest to observations to date, and the inability of the Control and SP to reproduce observations *is* likely a confirmation of unrealism and error.

4. Conclusions

We have focused primarily on surface flux response to precipitation and coupling scale. Surface-atmosphere interaction is bidirectional, and we expect coupling scale to influence precipitation characteristics. The large-scale moisture and temperature tendencies are constrained in this study to allow detailed evaluation of the land-atmosphere processes and how they control precipitation, canopy physiological function, and land-atmosphere flux. In HA10, it was demonstrated that replacing one land module with another that had been demonstrated competent at the K83 site in Brazil improved simulated representation of surface flux, planetary boundary layer thickness, and precipitation amount. Here, we take HA10 as a starting point and perform two experiments:

1. Replace the parameterized physics in the atmospheric model of HA10 with a "SP," or inclusion of a CRM, and
2. Investigate the influence of surface coupling scale on model behavior.

We find that replacing traditional GCM cloud and precipitation parameterizations results in a significant improvement in surface flux (latent and sensible heat) when compared against observations, and this improvement is not strongly dependent upon coupling scale. Monthly precipitation amount is well constrained in all three models but has significant differences with respect to intensity and frequency between models. The precipitation simulation is improved when the atmospheric model is changed from the Control to SP and improved further when coupling scale is decreased from ~100 to ~2 km in SP-X.

Additionally, coupling scale has significant influence on the fate of water with regard to what happens to precipitation once it encounters the canopy. The realistic simulation of more intense precipitation events provides an opportunity for water to run off leaves and become available for infiltration into the soil, where it can be stored and used to maintain transpiration (and photosynthesis) during dry months. The Control is always "playing catchup," in that even in the wet season, when soil moisture storage is being replenished, that process is inhibited in the Control by excessive radiation that evaporates water off of leaves and drives

transpiration. SP and SP-X, with more intense precipitation, more realistic radiation, and higher water vapor pressure in the canopy, have greater moisture storage in the soil.

The largest difference between SP and SP-X, as a result of coupling scale, is in the carbon-meteorology interactions. With the finer coupling scale (SP-X) we see more realistic behavior when compared to observed radiation-photosynthesis behavior on both the diurnal and seasonal scale. This suggests a more realistic simulation of mean seasonality.

The Control simulation, at the K83 site, shows a strong tendency toward water limitation (biotic control), while the MMF models sequentially tend toward light limitation (environmental control) as coupling scale decreases. This result does not lend itself to basin-wide predictions, as precipitation seasonality (annual total and dry season characteristics) is diverse. This study does shed some light on the processes involved in land-atmosphere coupling in tropical forest ecosystems, and how energy, moisture and carbon cycles are interconnected.

These results may have implications for simulations of global climate. Tropical South America teleconnects to global circulation (Avissar & Werth, 2005; Gedney & Valdes, 2000; Nobre et al., 2009; Werth, 2002), so we anticipate that changes in the simulation of carbon-climate feedbacks in this region may be reflected globally. Finally, a word of caution: The simulations here are driven with a reanalysis product (NCEP), and therefore, the temperature and moisture divergence forcing these SCMs are constrained. We cannot extrapolate the behavior explored here to different locations in climate and/or vegetation space. While the body of work describing simulations using first-generation MMF models (SP) is expanding it is possible, even likely, that coupling scale influence will have profound effects in a free-running global simulating using SP-X. This exploration provides exciting opportunities for future research.

A: Acronym List

- CESM-Community Earth System Model
- CRM-Cloud-resolving model
- EBF-Evergreen broadleaf forest
- ET-Evapotranspiration
- GCM-General Circulation Model
- GPP-Gross primary productivity (photosynthesis)
- H-Sensible Heat Flux
- LAI-Leaf area index
- LE-Latent Heat Flux
- MMF-Multiscale modeling framework
- NCEP-National Center for Environmental Prediction
- PDF-Probability density function
- RRTM-Rapid, accurate Radiative Transfer Model
- SCM-Single-column model
- SiB-Simple Biosphere Model
- SP-Superparameterization
- SP-X-Superparameterization with highly resolved surface coupling
- VPD-Vapor pressure deficit

Acknowledgments
This research was sponsored by NASA Contract NNX14AI52G, Department of Energy Contract DE-SC0014438, National Science Foundation Contract AGS-1049041, and National Science Foundation Science and Technology Center for Multi-Scale Modeling of Atmospheric Processes (CMMAP), managed by Colorado State University under cooperative agreement ATM-0425247. The K83 observational data are available from AmeriFlux (ameriflux.lbl.gov), NCEP Reanalysis data provided by NOAA/ESRL/PSD, Boulder, Colorado, USA, from the http://www.cdc.noaa.gov/ website. Model code and output is stored at GitLab (gitlab.com). This project is password protected, and the password can be obtained from the corresponding author at ian.baker@colostate.edu upon request.

References

Aït-Mesbah, S., Dufresne, J. L., Cheruy, F., & Hourdin, F. (2015). The role of thermal inertia in the representation of mean and diurnal range of surface temperature in semiarid and arid regions: Surface temperature in semiarid regions. *Geophysical Research Letters*, *42*, 7572–7580. https://doi.org/10.1002/2015GL065553

Araújo, A. C. (2002). Comparative measurements of carbon dioxide fluxes from two nearby towers in a central Amazonian rainforest: The Manaus LBA site. *Journal of Geophysical Research*, *107*(D20), 8090. https://doi.org/10.1029/2001JD000676

Avissar, R., & Werth, D. (2005). Global hydroclimatological teleconnections resulting from tropical deforestation. *Journal of Hydrometeorology*, *6*(2), 134–145. https://doi.org/10.1175/JHM406.1

Avitabile, V., Herold, M., Heuvelink, G. B. M., Lewis, S. L., Phillips, O. L., Asner, G. P., et al. (2016). An integrated pan-tropical biomass map using multiple reference datasets. *Global Change Biology*, *22*(4), 1406–1420. https://doi.org/10.1111/gcb.13139

Baker, I., Denning, A. S., Hanan, N., Prihodko, L., Uliasz, M., Vidale, P.-L., et al. (2003). Simulated and observed fluxes of sensible and latent heat and CO_2 at the WLEF-TV tower using SiB2.5. *Global Change Biology*, *9*(9), 1262–1277. https://doi.org/10.1046/j.1365-2486.2003.00671.x

Baker, I., Denning, S., & Stöckli, R. (2010). North American gross primary productivity: Regional characterization and interannual variability. *Tellus B: Chemical and Physical Meteorology*, *62*(5), 533–549. https://doi.org/10.1111/j.1600-0889.2010.00492.x

Baker, I., Harper, A., da Rocha, H., Denning, A., Araújo, A., Borma, L., et al. (2013). Surface ecophysiological behavior across vegetation and moisture gradients in tropical South America. *Agricultural and Forest Meteorology*, *182-183*, 177–188. https://doi.org/10.1016/j.agrformet.2012.11.015

Baker, I. T., Prihodko, L., Denning, A. S., Goulden, M., Miller, S., & da Rocha, H. R. (2008). Seasonal drought stress in the Amazon: Reconciling models and observations: TAPAJOS km 83 NEE ANNUAL CYCLE. *Journal of Geophysical Research*, *113*, G00B01. https://doi.org/10.1029/2007JG000644

Benedict, J. J., & Randall, D. A. (2009). Structure of the Madden–Julian Oscillation in the superparameterized CAM. *Journal of the Atmospheric Sciences*, *66*(11), 3277. https://doi.org/10.1175/2009JAS3030.1

Betts, R. A., Cox, P. M., Collins, M., Harris, P. P., Huntingford, C., & Jones, C. D. (2004). The role of ecosystem-atmosphere interactions in simulated Amazonian precipitation decrease and forest dieback under global climate warming. *Theoretical and Applied Climatology*, *78*(1-3), 157–175. https://doi.org/10.1007/s00704-004-0050-y

Betts, A., & Miller, M. (1986). A new convective adjustment scheme, Part II: Single column tests using GATE wave, BOMEX, ATEX and arctic air-mass data sets. *Quarterly Journal of the Royal Meteorological Society*, *112*(473), 693–709. https://doi.org/10.1256/smsqj.47307

Bonan, G. B. (2016). *Ecological climatology: Concepts and applications* (3rd ed.). New York: Cambridge University Press.

Clough, S., Shephard, M., Mlawer, E., Delamere, J., Iacono, M., Cady-Pereira, K., et al. (2005). Atmospheric radiative transfer modeling: A summary of the AER codes. *Journal of Quantitative Spectroscopy and Radiative Transfer*, *91*(2), 233–244. https://doi.org/10.1016/j.jqsrt.2004.05.058

Colello, G. D., Grivet, C., Sellers, P. J., & Berry, J. A. (1998). Modeling of energy, water, and CO $_2$ flux in a temperate grassland ecosystem with SiB2: May–October 1987. *Journal of the Atmospheric Sciences*, *55*(7), 1141–1169. https://doi.org/10.1175/1520-0469(1998)055<1141:MOEWAC>2.0.CO;2

Collatz, G., Ball, J., Grivet, C., & Berry, J. A. (1991). Physiological and environmental regulation of stomatal conductance, photosynthesis and transpiration: A model that includes a laminar boundary layer. *Agricultural and Forest Meteorology*, *54*(2-4), 107–136. https://doi.org/10.1016/0168-1923(91)90002-8

Collatz, G., Ribas-Carbo, M., & Berry, J. (1992). Coupled photosynthesis-stomatal conductance model for leaves of C_4 plants. *Australian Journal of Plant Physiology*, *19*(5), 519–538. https://doi.org/10.1071/PP9920519

Corbin, K., Denning, A., Lokupitiya, E., Schuh, A., Miles, N., Davis, K., et al. (2010). Assessing the impact of crops on regional CO_2 fluxes and atmospheric concentrations. *Tellus B: Chemical and Physical Meteorology*, *62*(5), 521–532. https://doi.org/10.1111/j.1600-0889.2010.00485.x

Costa, M. H., Biajoli, M. C., Sanches, L., Malhado, A. C. M., Hutyra, L. R., da Rocha, H. R., et al. (2010). Atmospheric versus vegetation controls of Amazonian tropical rain forest evapotranspiration: Are the wet and seasonally dry rain forests any different? *Journal of Geophysical Research*, *115*, G04021. https://doi.org/10.1029/2009JG001179

Couvreux, F., Guichard, F., Gounou, A., Bouniol, D., Peyrillé, P., & Köhler, M. (2014). Modelling of the thermodynamical diurnal cycle in the lower atmosphere: A joint evaluation of four contrasted regimes in the tropics over land. *Boundary-Layer Meteorology*, *150*(2), 185–214. https://doi.org/10.1007/s10546-013-9862-6

Cox, P. M., Betts, R. A., Collins, M., Harris, P. P., Huntingford, C., & Jones, C. D. (2004). Amazonian forest dieback under climate-carbon cycle projections for the 21st century. *Theoretical and Applied Climatology*, *78*(1-3), 137–156. https://doi.org/10.1007/s00704-004-0049-4

Cox, P. M., Betts, R. A., Jones, C. D., Spall, S. A., & Totterdell, I. J. (2000). Erratum: Acceleration of global warming due to carbon-cycle feedbacks in a coupled climate model. *Nature*, *408*(6809), 184–187. https://doi.org/10.1038/35041539

Cox, P. M., Pearson, D., Booth, B. B., Friedlingstein, P., Huntingford, C., Jones, C. D., & Luke, C. M. (2013). Sensitivity of tropical carbon to climate change constrained by carbon dioxide variability. *Nature*, *494*(7437), 341–344. https://doi.org/10.1038/nature11882

Cripe, D. G., & Randall, D. A. (2001). Joint variations of temperature and water vapor over the midlatitude continents. *Geophysical Research Letters*, *28*(13), 2613–2616. https://doi.org/10.1029/2001GL012909

da Rocha, H. R., Manzi, A. O., Cabral, O. M., Miller, S. D., Goulden, M. L., Saleska, S. R., et al. (2009). Patterns of water and heat flux across a biome gradient from tropical forest to savanna in Brazil. *Journal of Geophysical Research*, *114*, G00B12. https://doi.org/10.1029/2007JG000640

da Rocha, H., Nobre, C., Bonatti, J., Wright, I., & Sellers, P. J. (1996). A vegetation-atmosphere interaction study for Amazonia deforestation using field data and a 'single column' model. *Quarterly Journal of the Royal Meteorological Society*, *122*, 567–594.

Davidson, E. A., de Araújo, A. C., Artaxo, P., Balch, J. K., Brown, I. F., Bustamante, M. M. C., et al. (2012). The Amazon basin in transition. *Nature*, *481*(7381), 321–328. https://doi.org/10.1038/nature10717

Davies-Barnard, T., Valdes, P. J., Jones, C. D., & Singarayer, J. S. (2014). Sensitivity of a coupled climate model to canopy interception capacity. *Climate Dynamics*, *42*(7-8), 1715–1732. https://doi.org/10.1007/s00382-014-2100-1

de Gonçalves, L. G. G., Borak, J. S., Costa, M. H., Saleska, S. R., Baker, I., Restrepo-Coupe, N., et al. (2013). Overview of the Large-Scale Biosphere-Atmosphere Experiment in Amazonia Data Model Intercomparison Project (LBA-DMIP). *Agricultural and Forest Meteorology*, *182-183*, 111–127. https://doi.org/10.1016/j.agrformet.2013.04.030

DeMott, C. A., Randall, D. A., & Khairoutdinov, M. (2007). Convective precipitation variability as a tool for general circulation model analysis. *Journal of Climate*, *20*(1), 91–112. https://doi.org/10.1175/JCLI3991.1

DeMott, C. A., Stan, C., & Randall, D. A. (2013). Northward propagation mechanisms of the boreal summer intraseasonal oscillation in the ERA-Interim and SP-CCSM. *Journal of Climate*, *26*(6), 1973–1992. https://doi.org/10.1175/JCLI-D-12-00191.1

DeMott, C. A., Stan, C., Randall, D. A., Kinter, J. L., & Khairoutdinov, M. (2011). The Asian monsoon in the superparameterized CCSM and its relationship to tropical wave activity. *Journal of Climate*, *24*(19), 5134–5156. https://doi.org/10.1175/2011JCLI4202.1

Denning, A. S., Nicholls, M. E., Prihodko, L., Baker, I. T., Vidale, P. L., Davis, K. J., & Bakwin, P. (2003). Simulated variations in atmospheric CO_2 over a Wisconsin forest using a coupled ecosystem-atmosphere model. *Global Change Biology*, *9*(9), 1241–1250.

Dolman, A. J., & Gregory, D. (1992). The parametrization of rainfall interception in GCMs. *Quarterly Journal of the Royal Meteorological Society*, *118*(505), 455–467. https://doi.org/10.1256/smsqj.50503

Eltahir, E. A. B., & Bras, R. L. (1993a). Estimation of the fractional coverage of rainfall in climate models. *Journal of Climate*, *6*(4), 639–644. https://doi.org/10.1175/1520-0442(1993)006<0639:EOTFCO>2.0.CO;2

Eltahir, E. A. B., & Bras, R. L. (1993b). A description of rainfall interception over large areas. *Journal of Climate*, *6*(6), 1002–1008. https://doi.org/10.1175/1520-0442(1993)006<1002:ADORIO>2.0.CO;2

Entekhabi, D., & Eagleson, P. S. (1989). Land surface hydrology parameterization for atmospheric general circulation models including subgrid scale spatial variability. *Journal of Climate*, *2*(8), 816–831. https://doi.org/10.1175/1520-0442(1989)002<0816:LSHPFA>2.0.CO;2

Falge, E., Baldocchi, D., Tenhunen, J., Aubinet, M., Bakwin, P., Berbigier, P., et al. (2002). Seasonality of ecosystem respiration and gross primary production as derived from FLUXNET measurements. *Agricultural and Forest Meteorology*, *113*(1-4), 53–74. https://doi.org/10.1016/S0168-1923(02)00102-8

Farquhar, G. D., von Caemmerer, S., & Berry, J. A. (1980). A biochemical model of photosynthetic CO_2 assimilation in leaves of C_3 species. *Planta*, *149*(1), 78–90. https://doi.org/10.1007/BF00386231

Franks, S., Beven, K., Quinn, P., & Wright, I. (1997). On the sensitivity of soil-vegetation-atmosphere transfer (SVAT) schemes: Equifinality and the problem of robust calibration. *Agricultural and Forest Meteorology*, *86*(1-2), 63–75. https://doi.org/10.1016/S0168-1923(96)02421-5

Friedlingstein, P., Cox, P., Betts, R., Bopp, L., von Bloh, W., Brovkin, V., et al. (2006). Climate–carbon cycle feedback analysis: Results from the C ^{4} MIP model intercomparison. *Journal of Climate*, *19*(14), 3337–3353. https://doi.org/10.1175/JCLI3800.1

Friedlingstein, P., Meinshausen, M., Arora, V. K., Jones, C. D., Anav, A., Liddicoat, S. K., & Knutti, R. (2014). Uncertainties in CMIP5 climate projections due to carbon cycle feedbacks. *Journal of Climate*, *27*(2), 511–526. https://doi.org/10.1175/JCLI-D-12-00579.1

Fu, R., Zhu, B., & Dickinson, R. E. (1999). How do atmosphere and land surface influence seasonal changes of convection in the tropical Amazon? *Journal of Climate*, *12*(5), 1306–1321. https://doi.org/10.1175/1520-0442(1999)012<1306:HDAALS>2.0.CO;2

Ganzeveld, L., & Lelieveld, J. (2004). Impact of Amazonian deforestation on atmospheric chemistry: Deforestation and atmospheric chemistry. *Geophysical Research Letters*, *31*, L06105. https://doi.org/10.1029/2003GL019205

Gedney, N., & Valdes, P. J. (2000). The effect of Amazonian deforestation on the Northern Hemisphere circulation and climate. *Geophysical Research Letters*, *27*(19), 3053–3056. https://doi.org/10.1029/2000GL011794

Good, P., Gregory, J. M., Lowe, J. A., & Andrews, T. (2013). Abrupt CO_2 experiments as tools for predicting and understanding CMIP5 representative concentration pathway projections. *Climate Dynamics*, *40*(3-4), 1041–1053. https://doi.org/10.1007/s00382-012-1410-4

Goulden, M., Miller, S., da Rocha, H. R., Menton, M., de Freitas, H. C., Silva Figueroa, A., & de Sousa, C. (2004). Diel and seasonal patterns of tropical forest CO_2 exchange. *ECOLOGICAL APPLICATIONS*, *14*(4), S42—S54.

Grabowski, W. W., Bechtold, P., Cheng, A., Forbes, R., Halliwell, C., Khairoutdinov, M., et al. (2006). Daytime convective development over land: A model intercomparison based on LBA observations. *Quarterly Journal of the Royal Meteorological Society*, *132*(615), 317–344. https://doi.org/10.1256/qj.04.147

Guichard, F., Petch, J., Redelsperger, J.-L., Bechtold, P., Chaboureau, J.-P., Cheinet, S., et al. (2004). Modelling the diurnal cycle of deep precipitating convection over land with cloud-resolving models and single-column models. *Quarterly Journal of the Royal Meteorological Society*, *130*(604), 3139–3172. https://doi.org/10.1256/qj.03.145

Gurney, K. R., Baker, D., Rayner, P., & Denning, S. (2008). Interannual variations in continental-scale net carbon exchange and sensitivity to observing networks estimated from atmospheric CO_2 inversions for the period 1980 to 2005: Interannual variations in carbon. *Global Biogeochemical Cycles*, *22*, GB3025. https://doi.org/10.1029/2007GB003082

Gustafsson, D., Lewan, E., van den Hurk, B. J. J. M., Viterbo, P., Grelle, A., Lindroth, A., et al. (2003). Boreal forest surface parameterization in the ECMWF Model—1D test with NOPEX long-term data. *Journal of Applied Meteorology*, *42*(1), 95–112. https://doi.org/10.1175/1520-0450(2003)042<0095:BFSPIT>2.0.CO;2

Hanan, N. P., Berry, J. A., Verma, S. B., Walter-Shea, E. A., Suyker, A. E., Burba, G. G., & Denning, A. S. (2005). Testing a model of CO_2, water and energy exchange in Great Plains tallgrass prairie and wheat ecosystems. *Agricultural and Forest Meteorology*, *131*(3-4), 162–179. https://doi.org/10.1016/j.agrformet.2005.05.009

Harper, A. B., Denning, A. S., Baker, I. T., Branson, M. D., Prihodko, L., & Randall, D. A. (2010). Role of deep soil moisture in modulating climate in the Amazon rainforest: Deep soil moisture and amazon climate. *Geophysical Research Letters*, *37*, L05802. https://doi.org/10.1029/2009GL042302

Horel, J. D., Hahmann, A. N., & Geisler, J. E. (1989). An investigation of the annual cycle of convective activity over the tropical Americas. *Journal of Climate*, *2*(11), 1388–1403. https://doi.org/10.1175/1520-0442(1989)002<1388:AIOTAC>2.0.CO;2

Houghton, R. A., Lawrence, K. T., Hackler, J. L., & Brown, S. (2001). The spatial distribution of forest biomass in the Brazilian Amazon: A comparison of estimates. *Global Change Biology*, *7*(7), 731–746. https://doi.org/10.1046/j.1365-2486.2001.00426.x

Hsieh, W. C., Rosa, D., & Collins, W. D. (2013). Global dust simulations in the multiscale modeling framework: SPCAM for global dust simulation. *Journal of Advances in Modeling Earth Systems*, *5*, 15–31. https://doi.org/10.1029/2012MS000150

Hu, Y., Gao, X., Shuttleworth, W. J., Gupta, H., Mahfouf, J.-F., & Viterbo, P. (1999). Soil-moisture nudging experiments with a single-column version of the ECMWF model. *Quarterly Journal of the Royal Meteorological Society*, *125*(557), 1879–1902. https://doi.org/10.1256/smsqj.55718

Huete, A. R., Didan, K., Shimabukuro, Y. E., Ratana, P., Saleska, S. R., Hutyra, L. R., et al. (2006). Amazon rainforests green-up with sunlight in dry season. *Geophysical Research Letters*, *33*, L06405. https://doi.org/10.1029/2005GL025583

Huffman, G. J., Adler, R. F., Bolvin, D. T., & Gu, G. (2009). Improving the global precipitation record: GPCP Version 2.1. *Geophysical Research Letters*, *36*, L17808. https://doi.org/10.1029/2009GL040000

Huntingford, C., Fisher, R. A., Mercado, L., Booth, B. B., Sitch, S., Harris, P. P., et al. (2008). Towards quantifying uncertainty in predictions of Amazon 'dieback'. *Philosophical Transactions of the Royal Society B: Biological Sciences*, *363*(1498), 1857–1864. https://doi.org/10.1098/rstb.2007.0028

Huntzinger, D., Schwalm, C., Wei, Y., Cook, R., Michalak, A., Schaeffer, K., et al. (2018). NACP MsTMIP: Global 0.5-degree model outputs in standard format. Version 1.0, https://doi.org/10.3334/ORNLDAAC/1225

Iacono, M. J., Mlawer, E. J., Clough, S. A., & Morcrette, J.-J. (2000). Impact of an improved longwave radiation model, RRTM, on the energy budget and thermodynamic properties of the NCAR community climate model, CCM3. *Journal of Geophysical Research*, *105*(D11), 14,873–14,890. https://doi.org/10.1029/2000JD900091

Jarvis, P. G. (1976). The interpretation of the variations in leaf water potential and stomatal conductance found in canopies in the field. *Philosophical Transactions of the Royal Society B: Biological Sciences*, *273*(927), 593–610. https://doi.org/10.1098/rstb.1976.0035

Jensen, J. L. W. V. (1906). Sur les fonctions convexes et les inégalités entre les valeurs moyennes. *Acta Mathematica*, *30*(0), 175–193. https://doi.org/10.1007/BF02418571

Jin, J., Lu, S., Li, S., & Miller, N. L. (2010). Impact of land use change on the local climate over the Tibetan Plateau. *Advances in Meteorology*, *2010*, 1–6. https://doi.org/10.1155/2010/837480

Jipp, P., Nepstad, D. C., Cassel, D., & de Carvalho, C. (1998). Deep soil moisture storage and transpiration in forests and pastures in seasonally-dry Amazonia. *Climatic Change*, *39*, 255–272. https://doi.org/10.1023/A:1005308930871

Kalnay, E., Kanamitsu, M., Kistler, R., Collins, W., Deaven, D., Gandin, L., et al. (1996). The NCEP/NCAR 40-year reanalysis project. *Bulletin of the American Meteorological Society*, *77*(3), 437–471. https://doi.org/10.1175/1520-0477(1996)077<0437:TNYRP>2.0.CO;2

Keenan, T. F., Carbone, M. S., Reichstein, M., & Richardson, A. D. (2011). The model–data fusion pitfall: Assuming certainty in an uncertain world. *Oecologia*, *167*(3), 587–597. https://doi.org/10.1007/s00442-011-2106-x

Khairoutdinov, M. F., & Kogan, Y. L. (1999). A large eddy simulation model with explicit microphysics: Validation against aircraft observations of a stratocumulus-topped boundary layer. *Journal of the Atmospheric Sciences*, *56*(13), 2115–2131. https://doi.org/10.1175/1520-0469(1999)056<2115:ALESMW>2.0.CO;2

Khairoutdinov, M. F., & Randall, D. A. (2001). A cloud resolving model as a cloud parameterization in the NCAR Community Climate System Model: Preliminary results. *Geophysical Research Letters*, *28*(18), 3617–3620. https://doi.org/10.1029/2001GL013552

Khairoutdinov, M., Randall, D., & DeMott, C. (2005). Simulations of the atmospheric general circulation using a cloud-resolving model as a superparameterization of physical processes. *Journal of the Atmospheric Sciences*, *62*(7), 2136–2154. https://doi.org/10.1175/JAS3453.1

Kim, W., Arai, T., Kanae, S., Oki, T., & Musiake, K. (2001). Application of the Simple Biosphere Model(SiB2) to a paddy field for a period of growing season in GAME-tropics. *Journal of the Meteorological Society of Japan*, *79*(1B), 387–400. https://doi.org/10.2151/jmsj.79.387

Kooperman, G. J., Pritchard, M. S., Burt, M. A., Branson, M. D., & Randall, D. A. (2016). Robust effects of cloud superparameterization on simulated daily rainfall intensity statistics across multiple versions of the Community Earth System Model: Rainfall intensity statistics in SPCAM. *Journal of Advances in Modeling Earth Systems*, *8*, 140–165. https://doi.org/10.1002/2015MS000574

Laio, F., Porporato, A., Ridolfi, L., & Rodriguez-Iturbe, I. (2001). Plants in water-controlled ecosystems: Active role in hydrologic processes and response to water stress. *Advances in Water Resources*, *24*(7), 707–723. https://doi.org/10.1016/S0309-1708(01)00005-7

Lasslop, G., Reichstein, M., Papale, D., Richardson, A. D., Arneth, A., Barr, A., et al. (2010). Separation of net ecosystem exchange into assimilation and respiration using a light response curve approach: Critical issues and global evaluation: separation of NEE into GPP and RECO. *Global Change Biology*, *16*(1), 187–208. https://doi.org/10.1111/j.1365-2486.2009.02041.x

Lee, M.-I., Choi, I., Tao, W.-K., Schubert, S. D., & Kang, I.-S. (2010). Mechanisms of diurnal precipitation over the US Great Plains: A cloud resolving model perspective. *Climate Dynamics*, *34*(2-3), 419–437. https://doi.org/10.1007/s00382-009-0531-x

Lee, J.-E., Frankenberg, C., van der Tol, C., Berry, J. A., Guanter, L., Boyce, C. K., et al. (2013). Forest productivity and water stress in Amazonia: Observations from GOSAT chlorophyll fluorescence. *Proceedings of the Royal Society B: Biological Sciences*, *280*(1761), 20130,171–20130,171. https://doi.org/10.1098/rspb.2013.0171

Lenderink, G., Siebesma, A. P., Cheinet, S., Irons, S., Jones, C. G., Marquet, P., et al. (2004). The diurnal cycle of shallow cumulus clouds over land: A single-column model intercomparison study. *Quarterly Journal of the Royal Meteorological Society*, *130*(604), 3339–3364. https://doi.org/10.1256/qj.03.122

Lokupitiya, E., Denning, A. S., Schaefer, K., Ricciuto, D., Anderson, R., Arain, M. A., et al. (2016). Carbon and energy fluxes in cropland ecosystems: A model-data comparison. *Biogeochemistry*, *129*(1-2), 53–76. https://doi.org/10.1007/s10533-016-0219-3

Lokupitiya, R. S., Zupanski, D., Denning, A. S., Kawa, S. R., Gurney, K. R., & Zupanski, M. (2008). Estimation of global CO_2 fluxes at regional scale using the maximum likelihood ensemble filter. *Journal of Geophysical Research*, *113*, D20110. https://doi.org/10.1029/2007JD009679

Malhi, Y., Wood, D., Baker, T. R., Wright, J., Phillips, O. L., Cochrane, T., et al. (2006). The regional variation of aboveground live biomass in old-growth Amazonian forests. *Global Change Biology*, *12*(7), 1107–1138. https://doi.org/10.1111/j.1365-2486.2006.01120.x

McNider, R. T., Steeneveld, G. J., Holtslag, A. A. M., Pielke, R. A., Mackaro, S., Pour-Biazar, A., et al. (2012). Response and sensitivity of the nocturnal boundary layer over land to added longwave radiative forcing: Sensitivity of the NBL over land. *Journal of Geophysical Research*, *117*, D14106. https://doi.org/10.1029/2012JD017578

Miller, S., Goulden, M., Menton, M., da Rocha, H., de Freitas, H., Silva Figueroa, A., & de Sousa, C. (2004). Biometric and micrometeorological measurements of tropical forest carbon balance. *ECOLOGICAL APPLICATIONS*, *14*(4), S114—S126.

Miller, S. D., Goulden, M. L., Hutyra, L. R., Keller, M., Saleska, S. R., Wofsy, S. C., et al. (2011). Reduced impact logging minimally alters tropical rainforest carbon and energy exchange. *Proceedings of the National Academy of Sciences*, *108*(48), 19,431–19,435. https://doi.org/10.1073/pnas.1105068108

Miranda, E. J., Vourlitis, G. L., Filho, N. P., Priante, P. C., Campelo, J. H., Suli, G. S., et al. (2005). Seasonal variation in the leaf gas exchange of tropical forest trees in the rain forest–savanna transition of the southern Amazon Basin. *Journal of Tropical Ecology*, *21*(04), 451–460. https://doi.org/10.1017/S0266467405002427

Mlawer, E. J., Taubman, S. J., Brown, P. D., Iacono, M. J., & Clough, S. A. (1997). Radiative transfer for inhomogeneous atmospheres: RRTM, a validated correlated-k model for the longwave. *Journal of Geophysical Research*, *102*(D14), 16,663–16,682. https://doi.org/10.1029/97JD00237

Morton, D. C., Nagol, J., Carabajal, C. C., Rosette, J., Palace, M., Cook, B. D., et al. (2014). Amazon forests maintain consistent canopy structure and greenness during the dry season. *Nature*, *506*(7487), 221–224. https://doi.org/10.1038/nature13006

Muchow, R. C., & Sinclair, T. R. (1991). Water deficit effects on maize yields modeled under current and "greenhouse" climates. *Agronomy Journal*, *83*(6), 1052. https://doi.org/10.2134/agronj1991.00021962008300060023x

Nepstad, D. C., de Carvalho, C. R., Davidson, E. A., Jipp, P. H., Lefebvre, P. A., Negreiros, G. H., et al. (1994). The role of deep roots in the hydrological and carbon cycles of Amazonian forests and pastures. *Nature*, *372*(6507), 666–669. https://doi.org/10.1038/372666a0

Nicholls, M. E. (2004). A multiple-scale simulation of variations in atmospheric carbon dioxide using a coupled biosphere-atmospheric model. *Journal of Geophysical Research*, *109*, D18117. https://doi.org/10.1029/2003JD004482

Nieto-Ferreira, R., & Rickenbach, T. M. (2011). Regionality of monsoon onset in South America: A three-stage conceptual model. *International Journal of Climatology*, *31*(9), 1309–1321. https://doi.org/10.1002/joc.2161

Nobre, P., Malagutti, M., Urbano, D. F., de Almeida, R. A. F., & Giarolla, E. (2009). Amazon deforestation and climate change in a coupled model simulation. *Journal of Climate*, *22*(21), 5686–5697. https://doi.org/10.1175/2009JCLI2757.1

Oliveira, R. S., Bezerra, L., Davidson, E. A., Pinto, F., Klink, C. A., Nepstad, D. C., & Moreira, A. (2005). Deep root function in soil water dynamics in cerrado savannas of central Brazil. *Functional Ecology*, *19*(4), 574–581. https://doi.org/10.1111/j.1365-2435.2005.01003.x

Parazoo, N. C., Bowman, K., Frankenberg, C., Lee, J.-E., Fisher, J. B., Worden, J., et al. (2013). Interpreting seasonal changes in the carbon balance of southern Amazonia using measurements of XCO $_2$ and chlorophyll fluorescence from GOSAT: CARBON CYCLE OF SOUTHERN AMAZONIA. *Geophysical Research Letters*, *40*, 2829–2833. https://doi.org/10.1002/grl.50452

Peylin, P., Law, R. M., Gurney, K. R., Chevallier, F., Jacobson, A. R., Maki, T., et al. (2013). Global atmospheric carbon budget: Results from an ensemble of atmospheric CO_2 inversions. *Biogeosciences*, *10*(10), 6699–6720. https://doi.org/10.5194/bg-10-6699-2013

Pitman, A. J., Henderson-Sellers, A., & Yang, Z.-L. (1990). Sensitivity of regional climates to localized precipitation in global models. *Nature*, *346*(6286), 734–737. https://doi.org/10.1038/346734a0

Powell, T. L., Galbraith, D. R., Christoffersen, B. O., Harper, A., Imbuzeiro, H. M. A., Rowland, L., et al. (2013). Confronting model predictions of carbon fluxes with measurements of Amazon forests subjected to experimental drought. *New Phytologist*, *200*(2), 350–365. https://doi.org/10.1111/nph.12390

Pritchard, M. S., Bretherton, C. S., & DeMott, C. A. (2014). Restricting 32-128 km horizontal scales hardly affects the MJO in the Superparameterized Community Atmosphere Model v.3.0 but the number of cloud-resolving grid columns constrains vertical mixing. *Journal of Advances in Modeling Earth Systems*, *6*, 723–739. https://doi.org/10.1002/2014MS000340

Pritchard, M. S., Moncrieff, M. W., & Somerville, R. C. J. (2011). Orogenic propagating precipitation systems over the United States in a global climate model with embedded explicit convection. *Journal of the Atmospheric Sciences*, *68*(8), 1821–1840. https://doi.org/10.1175/2011JAS3699.1

Pritchard, M. S., & Somerville, R. C. J. (2009). Assessing the diurnal cycle of precipitation in a multi-scale climate model. *Journal of Advances in Modeling Earth Systems*, *2*, 12. https://doi.org/10.3894/JAMES.2009.1.12

Randall, D. A., & Cripe, D. G. (1999). Alternative methods for specification of observed forcing in single-column models and cloud system models. *Journal of Geophysical Research*, *104*(D20), 24,527–24,545. https://doi.org/10.1029/1999JD900765

Randall, D., Dazlich, D., Zhang, C., Denning, A., Sellers, P., Tucker, C., et al. (1996). A revised land surface parameterization (SiB2) for GCMS. Part III: The greening of the Colorado State University general circulation model. *Journal of Climate*, *9*(4), 738–763. https://doi.org/10.1175/1520-0442(1996)009<0738:ARLSPF>2.0.CO;2

Randall, D., Khairoutdinov, M., Arakawa, A., & Grabowski, W. (2003). Breaking the cloud parameterization deadlock. *Bulletin of the American Meteorological Society*, *84*(11), 1547–1564. https://doi.org/10.1175/BAMS-84-11-1547

Reichstein, M., Falge, E., Baldocchi, D., Papale, D., Aubinet, M., Berbigier, P., et al. (2005). On the separation of net ecosystem exchange into assimilation and ecosystem respiration: Review and improved algorithm. *Global Change Biology*, *11*(9), 1424–1439. https://doi.org/10.1111/j.1365-2486.2005.001002.x

Restrepo-Coupe, N., da Rocha, H. R., Hutyra, L. R., da Araujo, A. C., Borma, L. S., Christoffersen, B., et al. (2013). What drives the seasonality of photosynthesis across the Amazon basin? A cross-site analysis of eddy flux tower measurements from the Brasil flux network. *Agricultural and Forest Meteorology*, *182-183*, 128–144. https://doi.org/10.1016/j.agrformet.2013.04.031

Restrepo-Coupe, N., Levine, N. M., Christoffersen, B. O., Albert, L. P., Wu, J., Costa, M. H., et al. (2017). Do dynamic global vegetation models capture the seasonality of carbon fluxes in the Amazon basin? A data-model intercomparison. *Global Change Biology*, *23*(1), 191–208. https://doi.org/10.1111/gcb.13442

Rochetin, N., Lintner, B. R., Findell, K. L., Sobel, A. H., & Gentine, P. (2014). Radiative-convective equilibrium over a land surface. *Journal of Climate*, *27*(23), 8611–8629. https://doi.org/10.1175/JCLI-D-13-00654.1

Rödenbeck, C., Houweling, S., Gloor, M., & Heimann, M. (2003). CO_2 flux history 1982–2001 inferred from atmospheric data using a global inversion of atmospheric transport. *Atmospheric Chemistry and Physics*, *3*(6), 1919–1964. https://doi.org/10.5194/acp-3-1919-2003

Rutter, N., Essery, R., Pomeroy, J., Altimir, N., Andreadis, K., Baker, I., et al. (2009). Evaluation of forest snow processes models (SnowMIP2). *Journal of Geophysical Research*, *114*, D06111. https://doi.org/10.1029/2008JD011063

Saatchi, S. S., Houghton, R. A., Dos Santos Alvalá, R. C., Soares, J. V., & Yu, Y. (2007). Distribution of aboveground live biomass in the Amazon basin: AGLB in the Amazon basin. *Global Change Biology*, *13*(4), 816–837. https://doi.org/10.1111/j.1365-2486.2007.01323.x

Saleska, S. R. (2003). Carbon in Amazon forests: Unexpected seasonal fluxes and disturbance-induced losses. *Science*, *302*(5650), 1554–1557. https://doi.org/10.1126/science.1091165

Saleska, S. R., Didan, K., Huete, A. R., & Rocha, H. R. da (2007). Amazon forests green-up during 2005 drought. *Science*, *318*(5850), 612–612. https://doi.org/10.1126/science.1146663

Saleska, S. R., Wu, J., Guan, K., Araujo, A. C., Huete, A., Nobre, A. D., & Restrepo-Coupe, N. (2016). Dry-season greening of Amazon forests. *Nature*, *531*(7594), E4—E5. https://doi.org/10.1038/nature16457

Samanta, A., Ganguly, S., Hashimoto, H., Devadiga, S., Vermote, E., Knyazikhin, Y., et al. (2010). Amazon forests did not green-up during the 2005 drought: Amazon drought sensitivity. *Geophysical Research Letters*, *37*, L05401. https://doi.org/10.1029/2009GL042154

Samanta, A., Ganguly, S., & Myneni, R. B. (2011). MODIS enhanced vegetation index data do not show greening of Amazon forests during the 2005 drought. *New Phytologist*, *189*(1), 11–15. https://doi.org/10.1111/j.1469-8137.2010.03516.x

Sato, N., Sellers, P., Randall, D., Schneider, E., Shukla, J., Kinter, J., et al. (1989). Effects of implementing the simple biosphere model in a general circulation model. *Journal of the Atmospheric Sciences*, *46*(18), 2757–2782. https://doi.org/10.1175/1520-0469(1989)046<2757:EOITSB>2.0.CO;2

Schaefer, K., Collatz, G. J., Tans, P., Denning, A. S., Baker, I., Berry, J., et al. (2008). Combined Simple Biosphere/Carnegie-Ames-Stanford Approach terrestrial carbon cycle model. *Journal of Geophysical Research*, *113*, G03034. https://doi.org/10.1029/2007JG000603

Schaefer, K., Denning, A. S., & Leonard, O. (2004). The winter Arctic Oscillation and the timing of snowmelt in Europe: Arctic oscillation and snowmelt. *Geophysical Research Letters*, *31*, L22205. https://doi.org/10.1029/2004GL021035

Schaefer, K., Denning, A. S., Suits, N., Kaduk, J., Baker, I., Los, S., & Prihodko, L. (2002). Effect of climate on interannual variability of terrestrial CO_2 fluxes: Climate variability and terrestrial CO_2 fluxes. *Global Biogeochemical Cycles*, *16*(4), 1102. https://doi.org/10.1029/2002GB001928

Schuh, A. E., Denning, A. S., Corbin, K. D., Baker, I. T., Uliasz, M., Parazoo, N., et al. (2010). A regional high-resolution carbon flux inversion of North America for 2004. *Biogeosciences*, *7*(5), 1625–1644. https://doi.org/10.5194/bg-7-1625-2010

Schwalm, C. R., Williams, C. A., Schaefer, K., Anderson, R., Arain, M. A., Baker, I., et al. (2010). A model-data intercomparison of CO_2 exchange across North America: Results from the North American Carbon Program site synthesis. *Journal of Geophysical Research*, *115*, G00H05. https://doi.org/10.1029/2009JG001229

Sellers, P., Berry, J., Collatz, G., Field, C., & Hall, F. (1992). Canopy reflectance, photosynthesis, and transpiration. III. A reanalysis using improved leaf models and a new canopy integration scheme. *Remote Sensing of Environment*, *42*(3), 187–216. https://doi.org/10.1016/0034-4257(92)90102-P

Sellers, P. J., Bounoua, L., Collatz, G. J., Randall, D. A., Dazlich, D. A., Los, S. O., et al. (1996). Comparison of radiative and physiological effects of doubled atmospheric CO_2 on climate. *Science*, *271*(5254), 1402–1406. https://doi.org/10.1126/science.271.5254.1402

Sellers, P. J., Mintz, Y., Sud, Y. C., & Dalcher, A. (1986). A Simple Biosphere Model (SIB) for use within general circulation models. *Journal of the Atmospheric Sciences*, *43*(6), 505–531. https://doi.org/10.1175/1520-0469(1986)043<0505:ASBMFU>2.0.CO;2

Sellers, P., Randall, D., Collatz, G., Berry, J., Field, C., Dazlich, D., et al. (1996). A revised land surface parameterization (SiB2) for atmospheric GCMS. Part I: Model formulation. *Journal of Climate*, *9*(4), 676–705. https://doi.org/10.1175/1520-0442(1996)009<0676:ARLSPF>2.0.CO;2

Sellers, P. J., Tucker, C. J., Collatz, G. J., Los, S. O., Justice, C. O., Dazlich, D. A., & Randall, D. A. (1996). A revised land surface parameterization (SiB2) for atmospheric GCMS. Part II: The generation of global fields of terrestrial biophysical parameters from satellite data. *Journal of Climate*, *9*(4), 706–737. https://doi.org/10.1175/1520-0442(1996)009<0706:ARLSPF>2.0.CO;2

Shuttleworth, W. (1988a). Macrohydrology—The new challenge for process hydrology. *Journal of Hydrology*, *100*(1-3), 31–56. https://doi.org/10.1016/0022-1694(88)90180-1

Shuttleworth, W. J. (1988b). Evaporation from Amazonian rainforest. *Proceedings of the Royal Society B: Biological Sciences*, *233*(1272), 321–346. https://doi.org/10.1098/rspb.1988.0024

Stap, L. B., van den Hurk, B. J. J. M., van Heerwaarden, C. C., & Neggers, R. A. J. (2014). Modeled contrast in the response of the surface energy balance to heat waves for forest and grassland. *Journal of Hydrometeorology*, *15*(3), 973–989. https://doi.org/10.1175/JHM-D-13-029.1

Stephens, G. L., Gabriel, P. M., & Partain, P. T. (2001). Parameterization of atmospheric radiative transfer. Part I: Validity of simple models. *Journal of the Atmospheric Sciences*, *58*(22), 3391–3409. https://doi.org/10.1175/1520-0469(2001)058<3391:POARTP>2.0.CO;2

Sterk, H. A. M., Steeneveld, G. J., Bosveld, F. C., Vihma, T., Anderson, P. S., & Holtslag, A. A. M. (2016). Clear-sky stable boundary layers with low winds over snow-covered surfaces. Part 2: Process sensitivity: Stable Boundary Layers over Snow: Process Sensitivity. *Quarterly Journal of the Royal Meteorological Society*, *142*(695), 821–835. https://doi.org/10.1002/qj.2684

Stirling, A. J., & Stratton, R. A. (2012). Entrainment processes in the diurnal cycle of deep convection over land. *Quarterly Journal of the Royal Meteorological Society*, *138*(666), 1135–1149. https://doi.org/10.1002/qj.1868

Sušelj, K., Teixeira, J. a., & Matheou, G. (2012). Eddy diffusivity/mass flux and shallow cumulus boundary layer: An updraft PDF multiple mass flux scheme. *Journal of the Atmospheric Sciences*, *69*(5), 1513–1533. https://doi.org/10.1175/JAS-D-11-090.1

Svensson, G., Holtslag, A. A. M., Kumar, V., Mauritsen, T., Steeneveld, G. J., Angevine, W. M., et al. (2011). Evaluation of the diurnal cycle in the atmospheric boundary layer over land as represented by a variety of single-column models: The second GABLS experiment. *Boundary-Layer Meteorology*, *140*(2), 177–206. https://doi.org/10.1007/s10546-011-9611-7

Thayer-Calder, K., & Randall, D. A. (2009). The role of convective moistening in the Madden-Julian Oscillation. *Journal of the Atmospheric Sciences*, *66*(11), 3297–3312. https://doi.org/10.1175/2009JAS3081.1

Valentini, R., Matteucci, G., Dolman, A. J., Schulze, E.-D., Rebmann, C., Moors, E. J., et al. (2000). Respiration as the main determinant of carbon balance in European forests. *Nature*, *404*(6780), 861–865. https://doi.org/10.1038/35009084

Vidale, P. L., & Stöckli, R. (2005). Prognostic canopy air space solutions for land surface exchanges. *Theoretical and Applied Climatology*, *80*(2-4), 245–257. https://doi.org/10.1007/s00704-004-0103-2

von Randow, C., Manzi, A. O., Kruijt, B., de Oliveira, P. J., Zanchi, F. B., Silva, R. L., et al. (2004). Comparative measurements and seasonal variations in energy and carbon exchange over forest and pasture in South West Amazonia. *Theoretical and Applied Climatology*, *78*(1-3), 5–26. https://doi.org/10.1007/s00704-004-0041-z

Wang, J.-W., Denning, A. S., Lu, L., Baker, I. T., Corbin, K. D., & Davis, K. J. (2007). Observations and simulations of synoptic, regional, and local variations in atmospheric CO_2. *Journal of Geophysical Research*, *112*, D04108. https://doi.org/10.1029/2006JD007410

Wang, M., Ghan, S., Ovchinnikov, M., Liu, X., Easter, R., Kassianov, E., et al. (2011). Aerosol indirect effects in a multi-scale aerosol-climate model PNNL-MMF. *Atmospheric Chemistry and Physics*, *11*(11), 5431–5455. https://doi.org/10.5194/acp-11-5431-2011

Wenzel, S., Cox, P. M., Eyring, V., & Friedlingstein, P. (2014). Emergent constraints on climate-carbon cycle feedbacks in the CMIP5 Earth system models. *Journal of Geophysical Research: Biogeosciences*, *119*, 794–807. https://doi.org/10.1002/2013JG002591

Werth, D. (2002). The local and global effects of Amazon deforestation. *Journal of Geophysical Research*, *107*(D20), 8087. https://doi.org/10.1029/2001JD000717

Williams, I. N., Lu, Y., Kueppers, L. M., Riley, W. J., Biraud, S. C., Bagley, J. E., & Torn, M. S. (2016). Land-atmosphere coupling and climate prediction over the U.S. Southern Great Plains: Land-atmosphere coupling and climate. *Journal of Geophysical Research: Atmospheres*, *121*, 12,125–12,144. https://doi.org/10.1002/2016JD025223

Wohlfahrt, G., & Galvagno, M. (2017). Revisiting the choice of the driving temperature for eddy covariance CO 2 flux partitioning. *Agricultural and Forest Meteorology*, *237-238*, 135–142. https://doi.org/10.1016/j.agrformet.2017.02.012

Wu, J., Serbin, S. P., Xu, X., Albert, L. P., Chen, M., Meng, R., et al. (2017). The phenology of leaf quality and its within-canopy variation is essential for accurate modeling of photosynthesis in tropical evergreen forests. *Global Change Biology*, *23*(11), 4814–4827. https://doi.org/10.1111/gcb.13725

Zhang, C., Dazlich, D. A., Randall, D. A., Sellers, P. J., & Denning, A. S. (1996). Calculation of the global land surface energy, water and CO_2 fluxes with an off-line version of SiB2. *Journal of Geophysical Research*, *101*(D14), 19,061–19,075. https://doi.org/10.1029/96JD01449

Zhu, H., Hendon, H., & Jakob, C. (2009). Convection in a parameterized and superparameterized model and its role in the representation of the MJO. *Journal of the Atmospheric Sciences*, *66*(9), 2796–2811. https://doi.org/10.1175/2009JAS3097.1